

**THE RISE VELOCITY OF AN AIR BUBBLE IN COARSE POROUS MEDIA:
THEORETICAL STUDIES**

**A THESIS SUBMITTED TO
THE GRADUATE SCHOOL OF NATURAL AND APPLIED SCIENCES
OF
THE MIDDLE EAST TECHNICAL UNIVERSITY**

BY

ABDULLAH CİHAN

**IN PARTIAL FULFILLMENT OF THE REQUIREMENTS FOR THE DEGREE OF
MASTER OF SCIENCE
IN
THE DEPARTMENT OF GEOLOGICAL ENGINEERING**

JANUARY 2004

Approval of the Graduate School of Natural and Applied Sciences

Prof. Dr. Canan ÖZGEN

Director

I certify that this thesis satisfies all the requirements as a thesis for the degree of Master of Science.

Prof. Dr. Asuman TÜRKMENOĞLU

Head of Department

This is to certify that we have read this thesis and that in our opinion it is fully adequate, in scope and quality, as a thesis for the degree of Master of Science.

Prof Dr. M. Yavuz ÇORAPÇIOĞLU

Supervisor

Examining Committee Members

Prof Dr. M. Yavuz ÇORAPÇIOĞLU

Prof. Dr. Kahraman ÜNLÜ

Prof Dr. Nurkan KARAHANOĞLU

Assoc. Prof. Dr. M. Zeki ÇAMUR

Assoc. Prof. Dr. Serhat AKIN

ABSTRACT

THE RISE VELOCITY OF AN AIR BUBBLE IN COARSE POROUS MEDIA: THEORETICAL STUDIES

Cihan, Abdullah

M.S., Department of Geological Engineering

Supervisor: Prof. Dr. M. Yavuz ÇORAPÇIOĞLU

January 2004, 54 pages

The rise velocity of injected air phase from the injection point toward the vadose zone is a critical factor in in-situ air sparging operations. It has been reported in the literature that air injected into saturated gravel rises as discrete air bubbles in bubbly flow of air phase. The objective of this study is to develop a quantitative technique to estimate the rise velocity of an air bubble in coarse porous media. The model is based on the macroscopic balance equation for forces acting on a bubble rising in a porous medium. The governing equation incorporates inertial force, added mass force, buoyant force, surface tension and drag force that results from the momentum transfer between the phases. The momentum transfer terms take into account the viscous as well as the kinetic energy losses at high velocities. Analytical solutions are obtained for steady, quasi-steady, and accelerated bubble rise velocities. Results show that air bubbles moving up through a porous medium equilibrate after a short travel time and very

short distances of rise. It is determined that the terminal rise velocity of a single air bubble in an otherwise water saturated porous medium cannot exceed 18.5 cm/sec. The theoretical model results compared favorably with the experimental data reported in the literature. A dimensional analysis conducted to study the effect of individual forces indicates that the buoyant force is largely balanced by the drag force for bubbles with an equivalent radius of 0.2-0.5 cm. With increasing bubble radius, the dimensionless number representing the effect of the surface tension force decreases rapidly. Since the total inertial force is quite small, the accelerated bubble rise velocity can be approximated by the terminal velocity.

Keywords: Air bubble, bubbly flow, granular media, discrete airflow.

ÖZ

ÇAKILLI ORTAMLARDA BİR HAVA KABARCIĞININ YÜKSELİM HIZI: TEORİK ÇALIŞMALAR

Cihan, Abdullah

Yüksek Lisans, Jeoloji Mühendisliği Bölümü

Tez Yöneticisi: Prof. Dr. M. Yavuz ÇORAPÇIOĞLU

Ocak 2004, 54 sayfa

Yerinde hava enjeksiyonu çalışmalarında, enjekte edilen hava fazın enjeksiyon noktasından vadoz zona doğru olan yükselim hızı önemli bir etkindir. Literatürde, hava fazın kabarcıklı akımında, doymun çakıllı ortamlar içerisinde enjekte edilen havanın ayrı hava kabarcıkları olarak yükseldiği belirtilmiştir. Bu çalışmanın amacı, gözenekli ortamlarda bir hava kabarcığının yükselim hızını belirlemek için niceliksel bir yöntem geliştirmektir. Geliştirilen bu model gözenekli bir ortamda yükselen bir hava kabarcığı üzerine etki eden kuvvetler için makroskobik korunum eşitliğine dayanır. Elde edilen korunum eşitliği fazlar arasındaki momentum transferinden oluşan sürtünme kuvvetleri, yüzey gerilimi, kaldırma kuvveti, katma kütle ve hareket ettirici kuvvetleri içerir. Momentum transfer terimleri yüksek hızlardaki kinetik ve viskoz enerji kayıplarını hasaba katar. Analitik çözümler kararlı, yarı-kararlı ve kararsız durum hava kabarcığı yükselim hızları için elde edilmiştir. Elde edilen sonuçlara göre, çakıllı bir

ortamda yükselen bir hava kabarcığı çok kısa bir yükselim süresi ve uzaklığından sonra dengeye ulaşır. Suyu doygun çakıllı bir ortamda bir hava kabarcığının yükselim hızının 18.5 cm/s'den fazla olamayacağı belirlenmiştir. Teorik model sonuçları literatürdeki benzer bir ortamda elde edilen deneysel verilerle karşılaştırılmış ve uyumlu olduğu gözlenmiştir. Her bir kuvvetin etkisini belirlemek için yapılan boyut analizi eşdeğer yarıçapı 0.2-0.5 cm olan hava kabarcıkları için, kaldırma kuvvetinin büyük ölçüde sürtünme kuvveti ile dengelendiğini göstermiştir. Yüzey gerilimini belirten boyutsuz sayının büyüklüğü, azalan kabarcık yarıçapı ile artar. Toplam hareket ettirici kuvvet oldukça küçük olduğu için, hava kabarcığının terminal hız ile yükseldiği kabul edilebilir.

Anahtar sözcükler: Hava kabarcığı, kabarcıklı akım, taneli ortamlar, ayrı hava akımı.

ACKNOWLEDGEMENTS

I gratefully acknowledge that it is a highly rewarding experience gained by working under the supervision of Prof. Dr. M. Yavuz ÇORAPCIOĞLU. I sincerely thank to him for his help, encouragement and valuable advice since the beginning of my masters program.

I would also like to express my appreciation to my family and Pınar TÜRKBEY for their patience and support during my studies.

TABLE OF CONTENTS

	<i>Page</i>
ABSTRACT	iii
ÖZ.....	v
ACKNOWLEDGEMENTS.....	vii
TABLE OF CONTENTS.....	viii
LIST OF FIGURES	xi
CHAPTER	
1. INTRODUCTION	1
2. FORCES ACTING ON A BUBBLE IN POROUS MEDIA.....	3
3. STEADY STATE (TERMINAL) BUBBLE RISE VELOCITY	12
4. QUASI-STEADY STATE BUBBLE RISE VELOCITY.....	15
5. ACCELERATED BUBBLE RISE VELOCITY	20
5.1. Solution with the Local Acceleration Only.....	20
5.2. Solution Including the Convective Component of the Acceleration.....	24
6. QUANTIFICATION OF FORCES	32

7. DIMENSIONAL ANALYSIS.....	37
8. SUMMARY AND CONCLUDING REMARKS.....	45
REFERENCES.....	46
APPENDIX	
A. NOTATION.....	49
B. TERMINAL VELOCITY MEASUREMENT OF AN AIR BUBBLE IN COARSE POROUS MEDIA.....	52

LIST OF TABLES

TABLE	<i>Page</i>
2.1. Model parameters used	9
7.1. Results of dimensional analysis	41

LIST OF FIGURES

FIGURE	Page
2.1. (a) A non-spherical bubble rising through the pore space, (b) Idealized schematic diagram of a bubble in a porous medium with orthorhombic packing arrangement, and (c) Force balance on a bubble at equilibrium.	5
3.1. Comparison of theoretical rise velocities with the experimental data of Roosevelt and Corapcioglu [1998]	14
4.1. Quasi-steady bubble rise velocities as a function of column depth without the added mass force	17
4.2. Quasi-steady bubble rise velocities as a function of column depth with the added mass force.....	18
4.3. Normalized rise velocities at Quasi-steady state with and without the added mass force (AM).....	19
5.1. Variation of bubble rise velocities with time at locally unsteady state without the added mass force.....	22
5.2. Variation of bubble rise velocities with time at locally unsteady state with the added mass force	23
5.3. General trend of the unsteady state solution for $R_b=0.2$ cm (a) w/o added mass, (b) with added mass	27
5.4. General trend of the unsteady state solution for $R_b=0.3$ cm (a) w/o added mass, (b) with added mass	28

5.5. General trend of the unsteady state solution for $R_b=0.4$ cm (a) w/o added mass, (b) with added mass	29
5.6. General trend of the unsteady state solution for $R_b=0.5$ cm (a) w/o added mass, (b) with added mass	30
5.7. Normalized rise velocities at locally unsteady and unsteady flow conditions with and without the added mass force (AM)	31
6.1. External forces at steady state	34
6.2. Temporal variation of force ratios for (a) $R_b=0.2$ cm and (b) $R_b=0.3$ cm	35
6.3. Temporal variation of force ratios for (a) $R_b=0.4$ cm and (b) $R_b=0.5$ cm	36
7.1. Dimensionless numbers as functions of the equivalent bubble radius	42
7.2. Ratio of dimensionless number a) D_1/D_3 and b) D_2^1/D_3 as functions of the bubble Reynolds number, Re	43
7.3. Ratio of dimensionless number a) D_1/D_2 and b) $1/D_3$ as functions of the bubble Reynolds number, Re	44

CHAPTER 1

INTRODUCTION

The migration of air bubbles in porous media has been the subject matter of a wide variety of studies in the literature, such as air sparging, bioslurping, trench aeration, and up-flow operation of filter beds are among the applications reported.

The mode of transport of air in granular porous media can take place either in the form of discrete air channels or discrete air bubbles. Transition from channel to bubble flow occurs with increasing grain size at about 1-2 mm diameter [Brooks *et al.*, 1996]. A qualitative study of airflow patterns through a water-saturated porous medium was conducted by Ji *et al.* [1993]. Laboratory visualization experiments were performed in a Plexiglass tank using glass beads as the porous medium. The sizes of the beads were 4, 2, 0.75, 0.4, 0.3, and 0.2 mm in diameter, which represent a range from fine gravels to fine sands. The injection of air into the 4-mm beads resulted in bubbly flow, discrete air bubbles migrating upward through the porous medium. A dual airflow pattern of bubbles and channels occurred in the 2-mm beads. Ji *et al.* [1993] noted that distorted plume shapes are observed when the medium has a heterogeneous pattern. Wehrle [1990] found air rising as bubbles in soils that were reported as fine gravel with particle diameter 3 mm and medium gravel with particle diameter 6 mm.

Semer et al. [1998] reported that injected air in saturated fine gravel traveled in discrete bubble form free of preferential pathways. *Gvirtzman and Gorelick* [1992] and *Pankow et al.* [1993] have discussed aeration techniques in open wells or trenches backfilled with coarse gravels or pebbles.

Roosevelt and Corapcioglu [1998] presented an experimental technique to study the rise of air bubbles through a granular porous medium by using video photography. Compressed air is injected into the base of a glass column filled with 4-mm glass beads and the resulting bubble motion is recorded by a camcorder and still frames are captured and enhanced with an image analyzer. *Roosevelt and Corapcioglu's* [1998] work is the first study to measure the terminal velocity of an air bubble rising in a porous medium.

Methods for quantifying the discrete air phase migration are important to optimize and design in-situ air sparging and trench aeration systems to remediate groundwater contaminated with volatile organic compounds. The limitations in modeling the air sparging process made this technique dependent on empirically based methodology for the engineering design of in-situ systems. Realistic air sparging models must include discrete air movement in coarse gravel and pebble formations. The objective of this study is to present an analysis to quantify the rise velocity of an air bubble in an otherwise water-saturated porous medium. We take into consideration the spatial and transient nature of the rise velocity as well as the forces acting on the bubble. We compare the results of the model with experimental data of *Roosevelt and Corapcioglu* [1998] in terms of rise velocities and bubble radii.

CHAPTER 2

FORCES ACTING ON A BUBBLE IN POROUS MEDIA

The starting point in the formulation will be the balance equation for forces acting on a rising bubble

$$\Sigma F = \forall_b \frac{D}{Dt} (\rho_g u_b) \quad (2.1)$$

where ΣF is the sum of forces acting on an air bubble, \forall_b is the volume of the bubble, t is the time, ρ_g is the density of air and u_b is the bubble rise velocity.

Assuming that the stationary porous medium is homogeneous, isotropic, fully saturated with water, and the fluids (water and gas) are incompressible, equation (2.1) can be rewritten in the vertical x -direction as

$$\Sigma F = \frac{4}{3} \pi R_b^3 \rho_g \left(\frac{\partial u_b}{\partial t} + u_b \frac{\partial u_b}{\partial x} \right) \quad (2.2)$$

The first term within the parentheses in (2.2) is the local acceleration. The second term is the convective component of the acceleration. In (2.2), R_b is the bubble radius defined as the equivalent radius of a sphere with a volume equal to that of a bubble. However, as an air bubble rises in a porous medium, it stretches, squeezes

and takes a non-spherical shape to pass through the pores of different sizes as shown in Figure 2.1a. As a bubble rises through a porous medium, a part of its surface area is in contact with solids and the rest is in contact with the liquid phase filling the pore spaces. However, since a thin film of water between the bubble and solid grains is always present, we assume that the bubble is completely surrounded by water. In this study, we neglect pore-level bubble generation mechanisms such as snap-off and division due to consideration of a single air bubble. The interplay of bubble generation and coalescence mechanisms can be quite important when a group of bubbles migrate in series as bubble trains. It is assumed that as a single bubble moves through the pore space that constantly contracts and expands, the energy used to stretch the bubble through the expanding pores is completely recovered as the bubble squeezes through the pore throats [*Kovscek and Radke, 1994*].

In this study, we assume that gas in an air bubble is an incompressible fluid. The incompressibility of gas flow is hard to achieve because gas density varies with pressure and the nonzero flux on the surface results in a "slip flow" known as the Klinkenberg effect. However, there are some cases when the incompressibility of gas flow can be achieved. This happens when the flow inducing pressure difference is 20% or less. The Klinkenberg effect can be neglected when the solid phase of the porous medium consists of silts, sands, and gravels [*Massmann, 1989*].

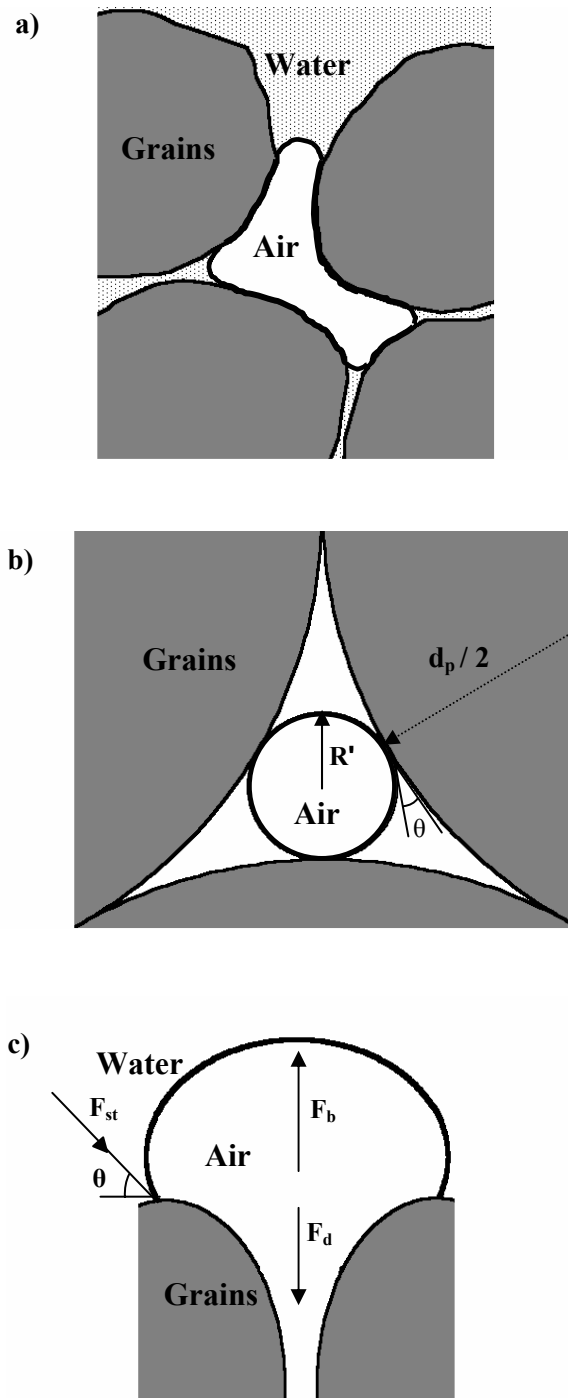


Figure 2.1. (a) A non-spherical bubble rising through the pore space, (b) Idealized schematic diagram of a bubble in a porous medium with orthorhombic packing arrangement, and (c) Force balance on a bubble at equilibrium.

The external forces acting on a bubble rising in an otherwise saturated porous medium result from gravitational effects (buoyancy), surface tension effects and drag forces. The expressions of individual mechanisms can be determined by either functional relations obtained through theoretical considerations or phenomenological equations. The Basset history force that results from the viscous effects generated by the acceleration of a particle relative to a fluid under the creeping flow conditions is neglected due to high bubble velocities [*Zhang and Fan, 2003*]. Due to irrotational flow conditions, we can also neglect the lift force acting on a bubble [*Soubiran and Sherwood, 2000*].

Density difference between the air and water results in upward buoyant force acting on an air bubble rising in water. The expression for the buoyant force, F_b is given by

$$F_b = (\rho_f - \rho_g) g \frac{4}{3} \pi R_b^3 \quad (2.3)$$

where ρ_f is the density of water.

The surface tension force results due to the difference between the inward attraction of the molecules inside the bubble and those at the contact surface of the bubble. In the vertical direction, it is expressed by

$$F_{st} = 2\pi R' \sigma \sin\theta \quad (2.4)$$

where σ is the surface tension, θ is the contact angle assumed to be constant during the bubble rise [Loubiere and Hebrard, 2003] and R' is the equivalent radius of a pore throat through which a bubble can pass in a particular arrangement of grains as shown in Figure 2.1b. Considering the equilibrium between the phases in a column of glass beads, θ is taken as 30° [Ortiz-Arroyo *et al.*, 2003]. Figure 2.1b shows the schematic diagram of a bubble in a porous medium with orthorhombic packing arrangement.

Since we plan to employ the data obtained by *Roosevelt and Corapcioglu* [1998] to test the validity of our mathematical model, we calculate R' based on a particular packing arrangement of spheres. *Roosevelt and Corapcioglu* [1998] used 4-mm glass beads in their column experiments. Ideal models based on uniform spheres are analogies of real porous media, which are very complex. Idealized glass bead models can be used to understand the various mechanisms and to investigate the forms of the governing equations as in our case. The relationship between R' and the particle diameter d_p can be calculated as $R' = (2\sqrt{3} - 3) d_p / 6$ for an orthorhombic arrangement.

One of the difficulties in modeling the flow through porous media is the expression of the momentum transfer terms that lead to drag forces. They require the characterization and solution of pore-scale equations. Assuming a simple periodic microstructure usually does this. After solving the pore-scale equations, the solutions are related to the macroscopic variables. An alternative approach is the use of empirical relations. In this study, due to the complexity of the pore-scale problem, we can approximate the interaction terms by assuming the validity of Darcy's law or similar expressions. If the theory formulated were for low

velocity problems, the assumption of laminar flow expressed by Darcy's law would be a reasonable one. However, for high velocity flow problems such as bubble rise, this may not be a valid assumption. Instead, the momentum transfer between the phases is due to kinetic as well as viscous energy losses. Since it incorporates both, the drag force acting on a bubble rising in a porous medium can be expressed by the modified Ergun (1952) equation. In Ergun's equation, the viscous energy losses are expressed by the Kozeny equation for laminar flow, proportional to the first power of the velocity, while the kinetic ones are expressed by the Burke-Plummer equation for turbulent flow, proportional to the product of density with the second power of the velocity. Then,

$$F_d = A \left[\frac{150 \mu_b u_b (1-n)^2}{d_p^2 n^3} + \frac{1.75 \rho_g u_b^2 (1-n)}{d_p n^3} \right] \frac{4}{3} \pi R_b^3 \quad (2.5)$$

where μ_b is the effective dynamic viscosity of the bubble, n is the porosity, d_p is the mean particle diameter, and A is the correction factor to incorporate the medium-specific surface properties as well as the partial contact of the bubble with solids as seen in Figure 2.1a. The effective dynamic viscosity of the bubble μ_b is expressed by *Kovscek and Radke* [1994] as $\mu_g + \alpha n_b / u_b^c$, where μ_g is the dynamic viscosity of air, α is the proportionality constant, n_b is the number of bubbles per unit volume of air, and c is an empirical constant. For a single bubble i.e., $n_b=1$, we find that $\mu_b \approx \mu_g$. Typical values of the model parameters are given in Table 2.1. The porosity of identical size randomly packed spheres

depends on the method of packing. The porosity of an orthorhombic arrangement as shown in Figure 2.1b is 0.3954 [Graton and Fraser, 1935]. This value of porosity is a typical one for gravel with spherical particles.

Table 2.1. Model parameters used

Parameters	Units	Values
μ_g	N.s/m ²	1.8×10^{-5}
μ_f	N.s/m ²	1×10^{-3}
ρ_g	kg/m ³	1.23
ρ_f	kg/m ³	997.3
σ	N/m	7.2×10^{-2}
g	m/s ²	9.81
n	%	39.54
d_p	m	0.004
α	Nm ^{7/3} s ^{2/3}	$4 \times 10^{-38/3}$
c		1/3

When a particle accelerates relative to the surrounding fluid, it creates a flow field possessing kinetic energy. Therefore an additional inertial force is needed to move the particle. Thus, the particle behaves as if it has an additional apparent mass equal to a ratio of the fluid mass that it displaces [Wallis, 1969]. The effect of additional “added mass” is an increase in the particular mass by $(C_M \rho_f / \rho_g)$ where the added mass coefficient, $C_M=11/16$ for a sphere moving in a fluid

normal to the wall [Loubiere and Hebrard, 2003]. Although this value of C_M is not a precise one for non-spherical bubbles; it was used in this study due to the lack of any other information available. For an ideal case of a sphere in an unbounded inviscid fluid $C_M = 1/2$ [Wallis, 1969]. The additional unit mass introduces an additional inertial unit force equal to $C_M \rho_f Du_b/Dt$.

Then, the force balance equation (2.2) is expressed as

$$\begin{aligned} (\rho_f - \rho_g)g \frac{4}{3} \pi R_b^3 - A \left[\frac{150 \mu_b u_b (1-n)^2}{d_p^2 n^3} + \frac{1.75 \rho_g u_b^2 (1-n)}{d_p n^3} \right] \frac{4}{3} \pi R_b^3 - \\ 2\pi R' \sigma \sin\theta = A_d \rho_g \frac{4}{3} \pi R_b^3 \left(\frac{\partial u_b}{\partial t} + u_b \frac{\partial u_b}{\partial x} \right) \end{aligned} \quad (2.6)$$

where $A_d = 1 + C_M \rho_f / \rho_g$.

In order to determine the solution of this equation in terms of bubble rise velocity, we will rearrange this equation to lump the terms with the same exponent of u_b .

$$-\left(C_1 u_b^2 + C_2 u_b + C_3 \right) = \frac{\partial u_b}{\partial t} + u_b \frac{\partial u_b}{\partial x} \quad (2.7)$$

where C_1 , C_2 , and C_3 are constant coefficients expressed by

$$C_1 = \frac{1.75A(1-n)}{d_p n^3 A_d} \quad (2.8)$$

$$C_2 = \frac{150A\mu_b(1-n)^2}{d_p^2 n^3 \rho_g A_d} \quad (2.9)$$

$$C_3 = \frac{1}{\rho_g A_d} \left[\frac{3}{2} \frac{R' \sigma \sin \theta}{R_b^3} - (\rho_f - \rho_g)g \right] \quad (2.10)$$

Equation (2.6) provides a general equation for an air bubble rising in an otherwise water saturated porous medium. Based on this equation, three different models describing the rise velocity of the bubble can be obtained:

- 1) Steady state motion in which the bubble rise velocity u_b does not explicitly change with time, that is $Du_b/Dt = 0$ in (2.1), and $A_d=1$ in (2.8)- (2.10).
- 2) Quasi-steady state motion in which the bubble rise velocity change with time is small i.e., $Du_b/Dt \cong u_b \partial u_b / \partial x$,
- 3) Unsteady state motion in which the bubble rise velocity changes with time.

The following sections present the analytical solutions of the balance equation for steady, quasi-steady, and for two forms of accelerated flow (unsteady state with local acceleration only and unsteady state including the convective component of the acceleration).

CHAPTER 3

STEADY STATE (TERMINAL) BUBBLE RISE VELOCITY

The steady state force balance equation of an air bubble in a porous medium is expressed by taking the right hand side of (2.6) equal to zero.

$$\begin{aligned} (\rho_f - \rho_g)g \frac{4}{3}\pi R_b^3 - A \left[\frac{150\mu_b u_b (1-n)^2}{d_p^2 n^3} + \right. \\ \left. \frac{1.75\rho_g u_b^2 (1-n)}{d_p n^3} \right] \frac{4}{3}\pi R_b^3 - 2\pi R' \sigma \sin\theta = 0 \end{aligned} \quad (3.1)$$

Then, the terminal bubble rise velocity is obtained as

$$\begin{aligned} u_b = \frac{\mu_b (1-n)}{\rho_g d_p} \left[-42.86 \pm \right. \\ \left. \sqrt{1836.74 - \frac{0.57}{A} \left(\frac{\rho_g d_p^3 n^3}{\mu_b^2 (1-n)^3} \right) \left(\frac{3 R'}{2 R_b^3} \sigma \sin\theta - (\rho_f - \rho_g)g \right)} \right] \end{aligned} \quad (3.2)$$

where A is the medium specific parameter determined as 26.8 by matching the experimental data. Traditionally, the equation (11) is solved inversely by using the experimental bubble velocities and then the correction factor A was obtained as an average value for corresponding bubble radii.

Only the solution in (3.2) with a positive sign represents the terminal bubble rise velocity. As seen in Figure 3.1, the comparison of the theoretical terminal bubble rise velocities given by (3.2) with the experimental data of *Roosevelt and Corapcioglu* [1998] shows a very favorable match for bubbles $R_b \geq 0.2$ cm. By employing the parameters given in Table 2.1, we can calculate from (3.2) that the terminal rise velocity of a single air bubble in an otherwise water saturated porous medium cannot exceed 18.5 cm/sec even when the effect of surface tension is neglected. Similarly, *Levich* [1962] has determined that the rise velocity of a single air bubble in a stationary water phase cannot exceed 30 cm/sec.

The experimental study conducted by *Roosevelt and Corapcioglu* [1998] observed that single bubbles might become stuck in a randomly packed homogeneous medium due to the changes in pore throat size. Nevertheless, *Roosevelt and Corapcioglu* [1998] obtained single bubbles traveling alone and free from any significant interactions with entrapped air. When the surface tension force is equal to the driving buoyant force, the bubble is trapped among the beads. Then the limiting pore throat radius can be calculated as

$$R' = \frac{2(\rho_f - \rho_g)gR_b^3}{3\sigma \sin\theta}$$

Roosevelt and Corapcioglu [1998] has noted in their experiments that the terminal travel distance of single bubble is quite short. Single bubbles often becomes stuck, trapped among the beads, and do not reach the top of the 1-m column. Occasionally, a single bubble will split into two bubbles because of collisions

with the porous medium. A rising bubble does, at times, move significantly in a lateral direction if the immediate vertical path is either blocked or too small. It may even move from one side of the column to the other. Nevertheless, *Roosevelt and Corapcioglu* [1998] found this type of motion to have a minimal effect on the average rise velocity.

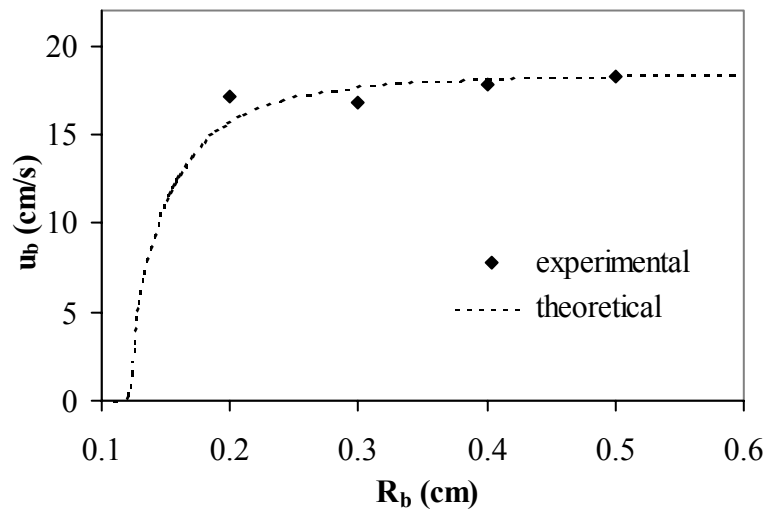


Figure 3.1. Comparison of theoretical rise velocities with the experimental data of *Roosevelt and Corapcioglu* [1998]

CHAPTER 4

QUASI-STEADY STATE BUBBLE RISE VELOCITY

Since the quasi-steady state includes only the convective term of the total acceleration, the balance equation (2.7) in a quasi-steady state is expressed by

$$C_1 u_b^2 + C_2 u_b + C_3 = -u_b \frac{du_b}{dx} \quad (4.1)$$

The solution of this equation can be obtained by employing the boundary condition at the base of the column i.e., $u_b = 0$ at $x = 0$. In this case, the column is a semi-infinite one. Then, the solution of the balance equation (4.1) is expressed by

$$x = \frac{C_2 - \sqrt{C_2^2 - 4C_1C_3}}{2C_1\sqrt{C_2^2 - 4C_1C_3}} \ln \left(\frac{2C_1u_b + C_2 - \sqrt{C_2^2 - 4C_1C_3}}{C_2 - \sqrt{C_2^2 - 4C_1C_3}} \right) - \frac{C_2 + \sqrt{C_2^2 - 4C_1C_3}}{2C_1\sqrt{C_2^2 - 4C_1C_3}} \ln \left(\frac{2C_1u_b + C_2 + \sqrt{C_2^2 - 4C_1C_3}}{C_2 + \sqrt{C_2^2 - 4C_1C_3}} \right) \quad (4.2)$$

The graphical representation of the solution (4.2) for different bubble radii with and without the effect of added mass is given in Figures 4.1 and 4.2. It can be seen

from the Figures that as the bubble radius increases, so does the rise velocity. Since the rise velocity approaches the steady state over a very short distance of rise, the convective component of the total acceleration can be neglected for practical purposes.

Another representation of the solution normalized by a reference, i.e., respective terminal velocities, $u_{ref}(R_b)$, which is the demonstration of the inclusion of the added mass force, is shown in Figure 4.3. As seen in Figure 4.3, the effect of added mass force is quite significant. Due to the high-density ratio of water to air, the bubble rise is retarded by an order of 500 ($A_d = 1 + C_M \rho_f / \rho_g = 558$) when the effect of added mass force is taken into consideration. For example, by neglecting the effect of added mass (i.e., $C_M = 0$), we calculate that a bubble with $R_b = 0.2$ cm reaches the terminal rise velocity at 0.0056 cm while the inclusion of added mass force increases the distance needed to reach the terminal velocity to 2.79 cm. Therefore A_d can be characterized as the “terminal velocity delay index” for bubble motion. In general, we can conclude that a distance of few bubble radii is needed to reach the terminal rise velocity. *Garrettson* [1973] obtained similar results for bubbles in the upper ocean.

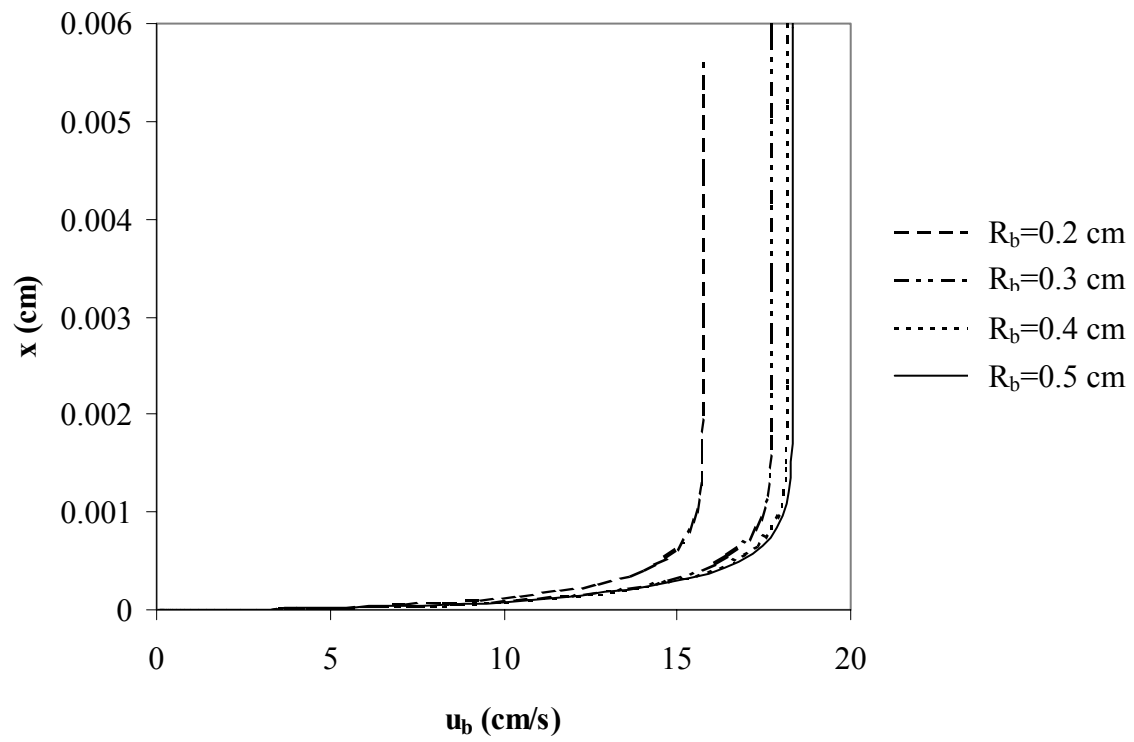


Figure 4.1. Quasi-steady bubble rise velocities as a function of column depth without the added mass force

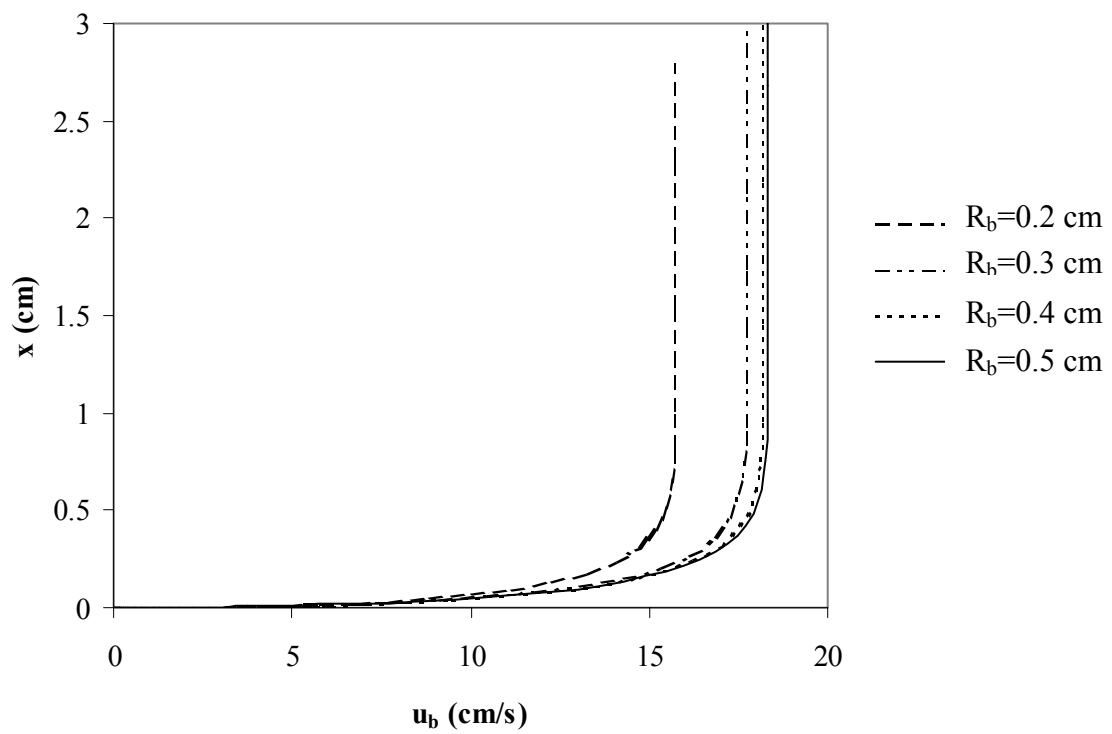


Figure 4.2. Quasi-steady bubble rise velocities as a function of column depth with the added mass force

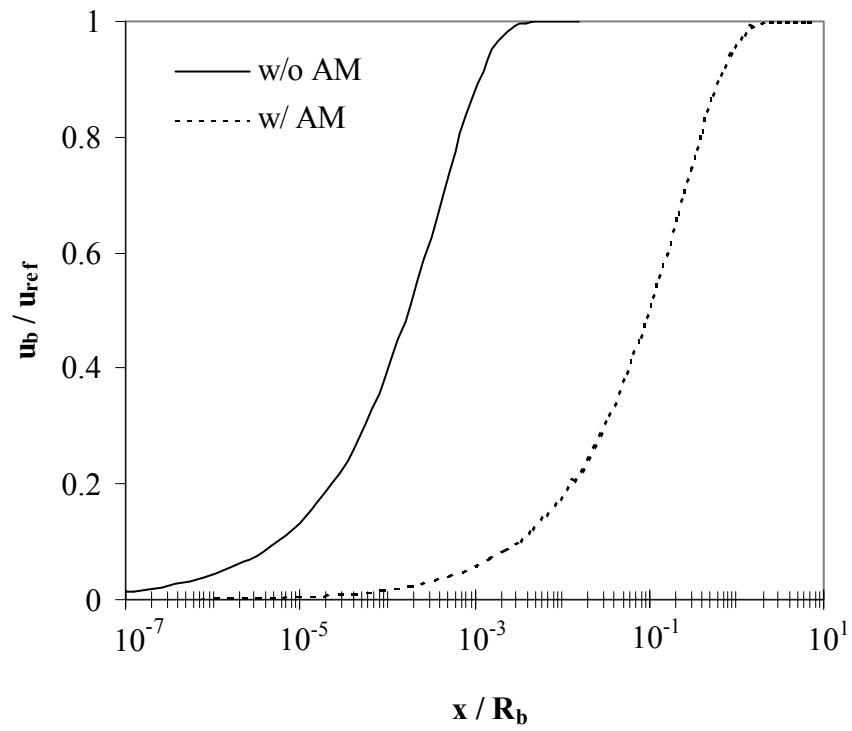


Figure 4.3. Normalized rise velocities at Quasi-steady state with and without the added mass force (AM)

CHAPTER 5

ACCELERATED BUBBLE RISE VELOCITY

The accelerated motion of an air bubble rising through a column of porous medium under unsteady state flow conditions can be expressed in two different forms: unsteady state with local term of acceleration only and unsteady state including the convective term in addition to the local acceleration. For both cases, the bubble is initially assumed to be a sphere with an equivalent radius R_b starting to rise at rest i.e., $u_b = 0$ at $t=0$ at the base of a column ($x=0$) as in the experiments of *Roosevelt and Corapcioglu* [1998].

5.1. Solution with the Local Acceleration Only

As defined earlier, in this type of unsteady state motion, the bubble rise velocity changes with time only. In this case, the velocity changes minimally with space i.e., the convective term of total acceleration is negligible. Then, the balance equation (2.7) is expressed as

$$C_1 u_b^2 + C_2 u_b + C_3 = -\frac{du_b}{dt} \quad (5.1)$$

where C_1 , C_2 and C_3 are given by (2.8)-(2.10), respectively. Then, the solution of (5.1) subject to the initial condition $u_b=0$ at $t=0$ is

$$u_b(t) = - \frac{2C_3 \tanh\left[\left(\frac{1}{2}\sqrt{C_2^2 - 4C_1C_3}\right)t\right]}{\left(\sqrt{C_2^2 - 4C_1C_3}\right) + C_2 \tanh\left[\left(\frac{1}{2}\sqrt{C_2^2 - 4C_1C_3}\right)t\right]} \quad (5.2)$$

The solution given by (5.2) is plotted in Figures 5.1 and 5.2 without and with incorporating the effect of added mass force, respectively. Both Figures show that larger bubbles have higher rise velocities. As seen in Figure 5.2, time to terminal velocity is delayed due to the effect of added mass force. In addition, it is seen from Figure 5.1 and 5.2 that the terminal velocity difference among the bubbles $R_b > 0.2$ tends to decrease. Terminal velocity of a bubble does not exceed 18.5 cm/sec however larger R_b becomes, which is the same result obtained in Chapter 3.

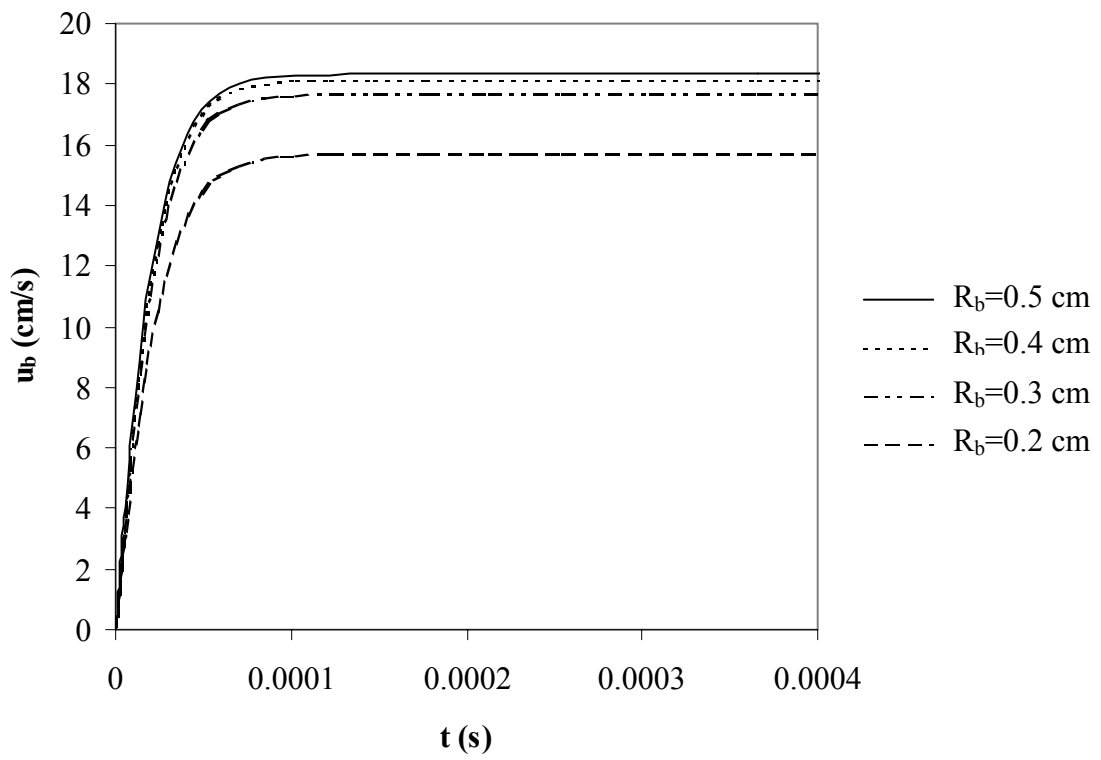


Figure 5.1. Variation of bubble rise velocities with time at locally unsteady state without the added mass force

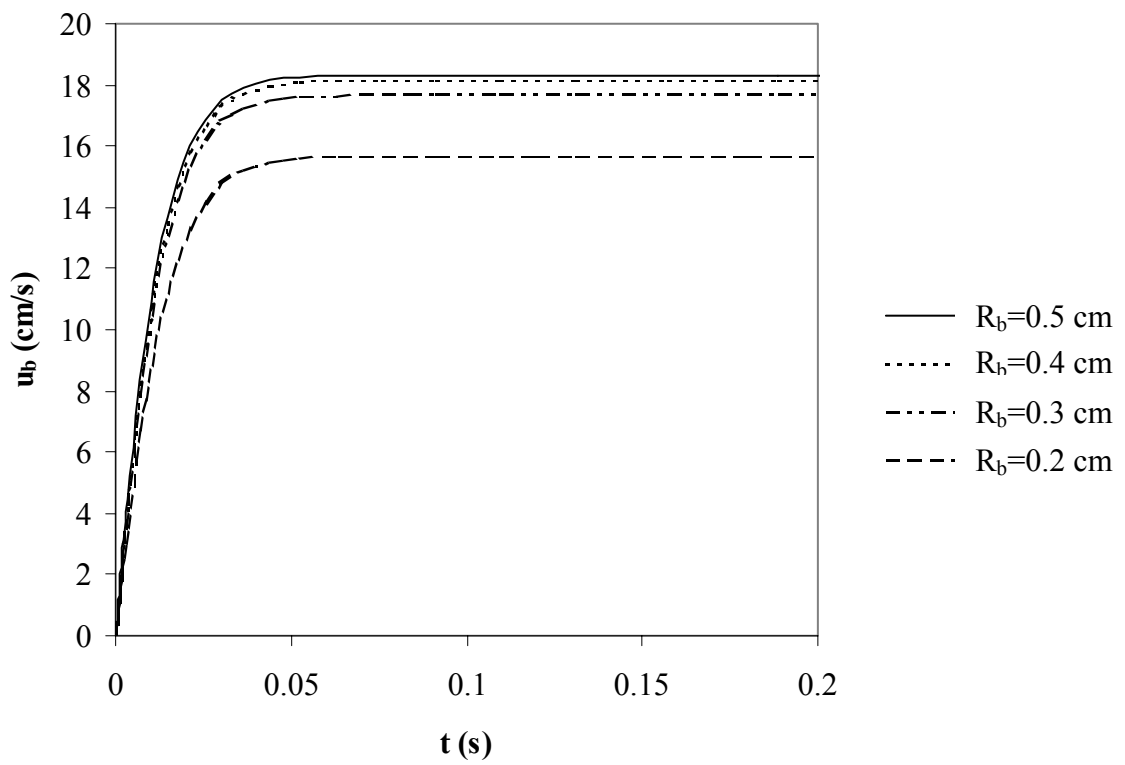


Figure 5.2. Variation of bubble rise velocities with time at locally unsteady state with the added mass force

5.2. Solution Including the Convective Component of the Acceleration

When the spatial variation of the rise velocity is taken into account as well as the temporal variation, then the solution of (2.7) can be obtained by applying the method of characteristics. Then,

$$dt = \frac{dx}{u_b} = - \frac{du_b}{(C_1 u_b^2 + C_2 u_b + C_3)} \quad (5.3)$$

Equation (5.3) shows that the general solution of equation (2.7) is $u_b(x,t) = f(x - u_b t)$ where the differentiable arbitrary function $f(x)$ is determined by the initial condition. From equation (5.3), we obtain two characteristics. The first characteristic $x(u_b)$, which is actually the quasi-steady state solution given by (4.2), expresses the variation of the bubble rise velocity along the column. The second characteristic, $t(u_b)$ is obtained by solving (2.7) subject to the initial condition $u_b = 0$ at $t = 0$. The characteristic $t(u_b)$ is obtained as

$$t = \frac{1}{\sqrt{C_2^2 - 4C_1C_3}} \left[\ln \left(\frac{2C_1u_b + C_2 + \sqrt{C_2^2 - 4C_1C_3}}{C_2 + \sqrt{C_2^2 - 4C_1C_3}} \right) - \ln \left(\frac{2C_1u_b + C_2 - \sqrt{C_2^2 - 4C_1C_3}}{C_2 - \sqrt{C_2^2 - 4C_1C_3}} \right) \right] \quad (5.4)$$

The characteristic $t(u_b)$ presents the temporal variation of the rise velocity. The solution of equation (2.7) is obtained by finding the intersection of the characteristics presented by equations (4.2) and (5.4) as

$$u_b(x,t) = -\frac{C_2 - \sqrt{C_2^2 - 4C_1C_3}}{2C_1} \left\{ 1 - \exp \left[-\frac{2C_1x + \left(C_2 + \sqrt{C_2^2 - 4C_1C_3} \right) t}{2} \right] \right\} \quad (5.5)$$

Demonstration of the solution (5.5) for all bubble radii is given in Figures 5.3-5.6. Figures show that the rise velocity of the bubbles with the equivalent radius $R_b=0.2-0.4$ cm arrives at the steady state after a short travel time and short distances of rise. Although the general trend of the solution seems to be similar for all bubbles, both time and distance to reach the terminal velocity is retarded when the added mass force is taken into account (Figures 5.3b, 5.4b, 5.5b, 5.6b).

The graphical representation of both (5.2) and (5.5) normalized by a reference rise velocity i.e., terminal velocity, $u_{ref}(R_b)$ were plotted in Figure 5.7 as functions of a dimensionless time variable ($t^* = t u_{ref} / R_b$). A comparison of (5.2) and (5.5) shows that there is practically no difference between these two solutions when the convective component of the acceleration is included. In another words, the temporal variations of the rise velocities are almost identical with both solutions. For example, at a distance of $x=0.00001$ cm, a bubble with $R_b=0.2$ cm reaches the terminal rise velocity at $t=0.00035$ sec with the local acceleration term only while the time to reach equilibrium increases to $t=0.0004$

sec when the convective component of acceleration is included in the total acceleration term. This is a difference that can be neglected for all practical purposes. However, the travel times to equilibrate shows an approximately 500-fold increase i.e., $t=0.2$ sec with the convective component of the acceleration when the effect of added mass is included in the formulation, a result similar to the one obtained under quasi-steady state conditions. The velocity lag caused by the added mass force is proportional to A_d .

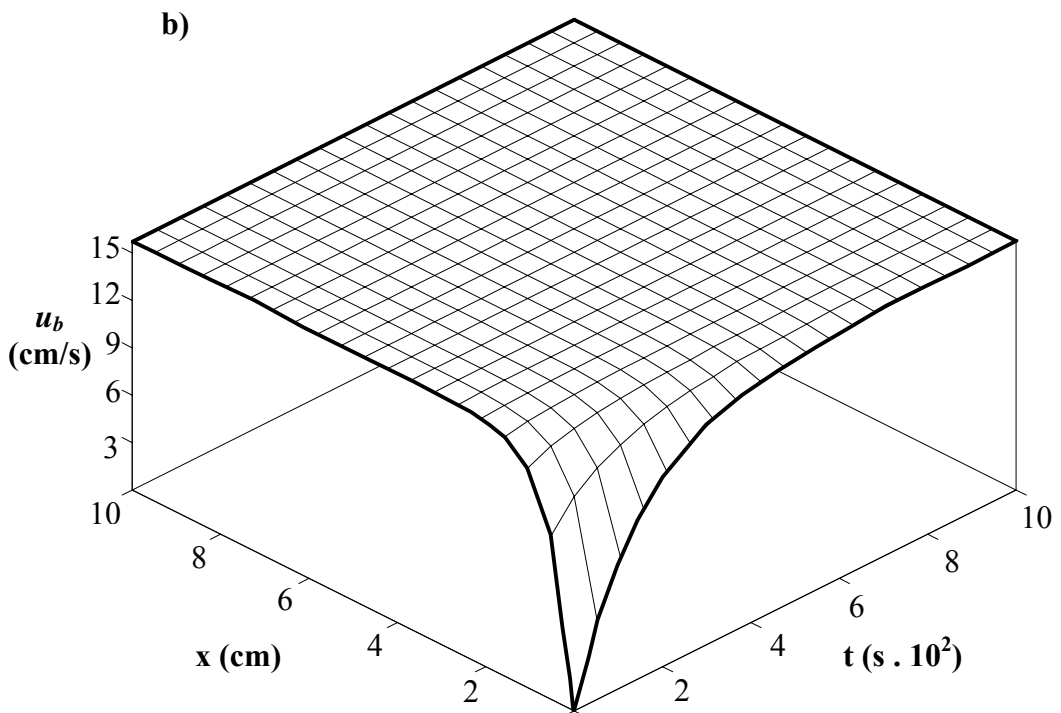
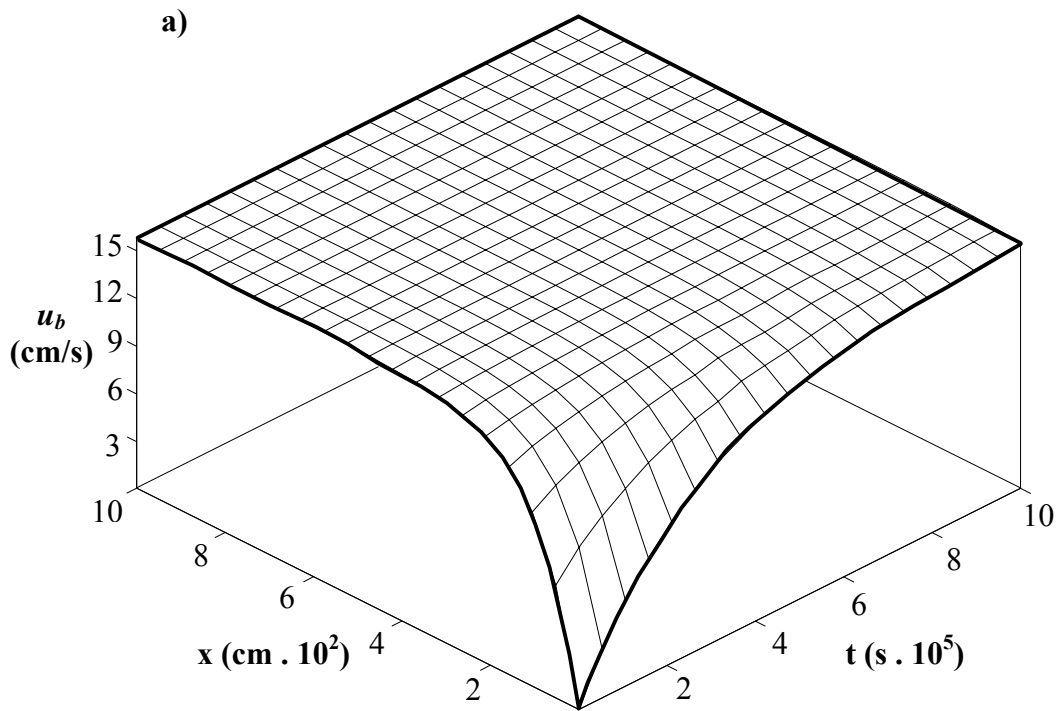


Figure 5.3. General trend of the unsteady state solution for $R_b=0.2$ cm (a) w/o added mass, (b) with added mass

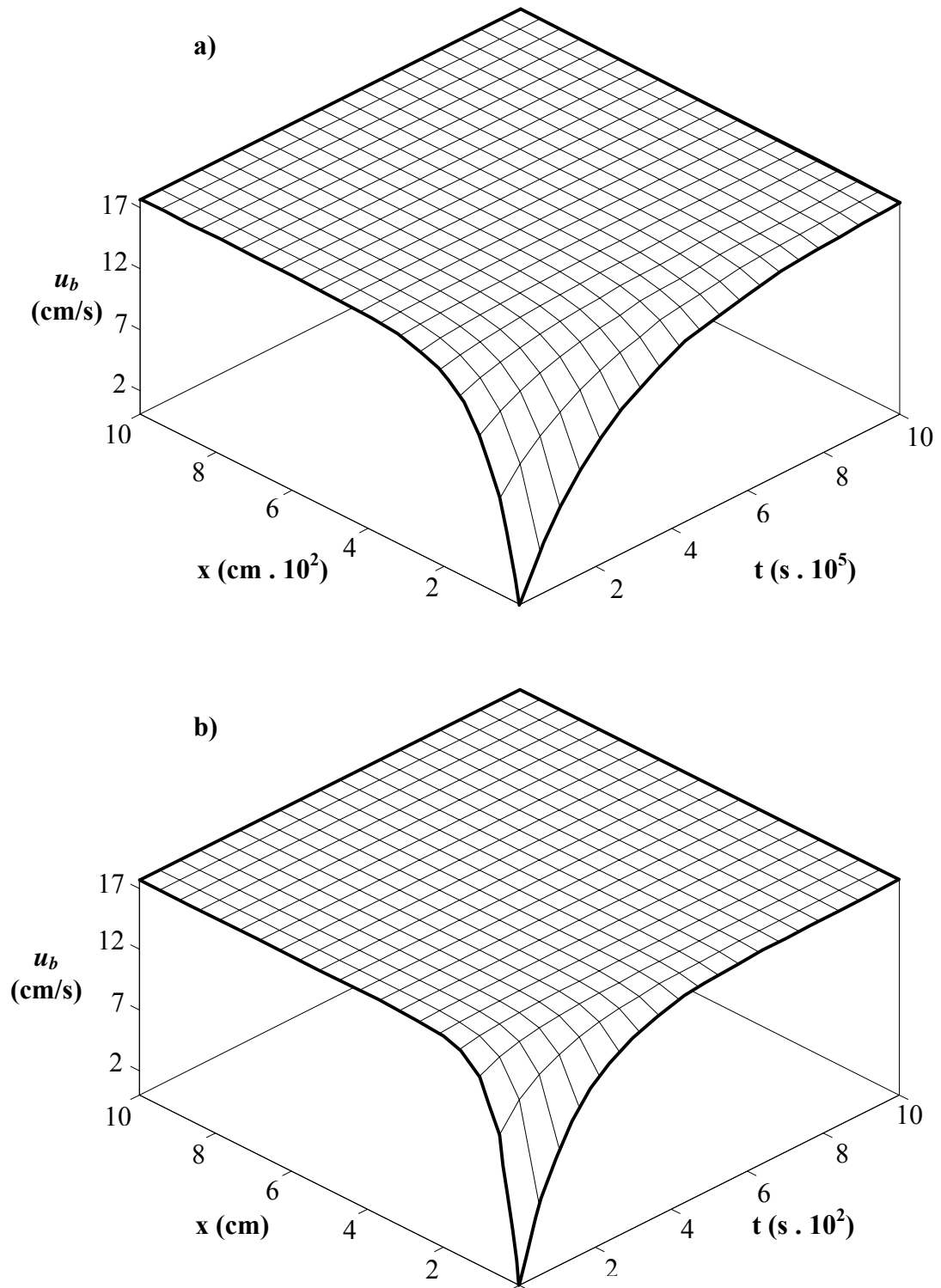


Figure 5.4. General trend of the unsteady state solution for $R_b=0.3$ cm (a) w/o added mass, (b) with added mass

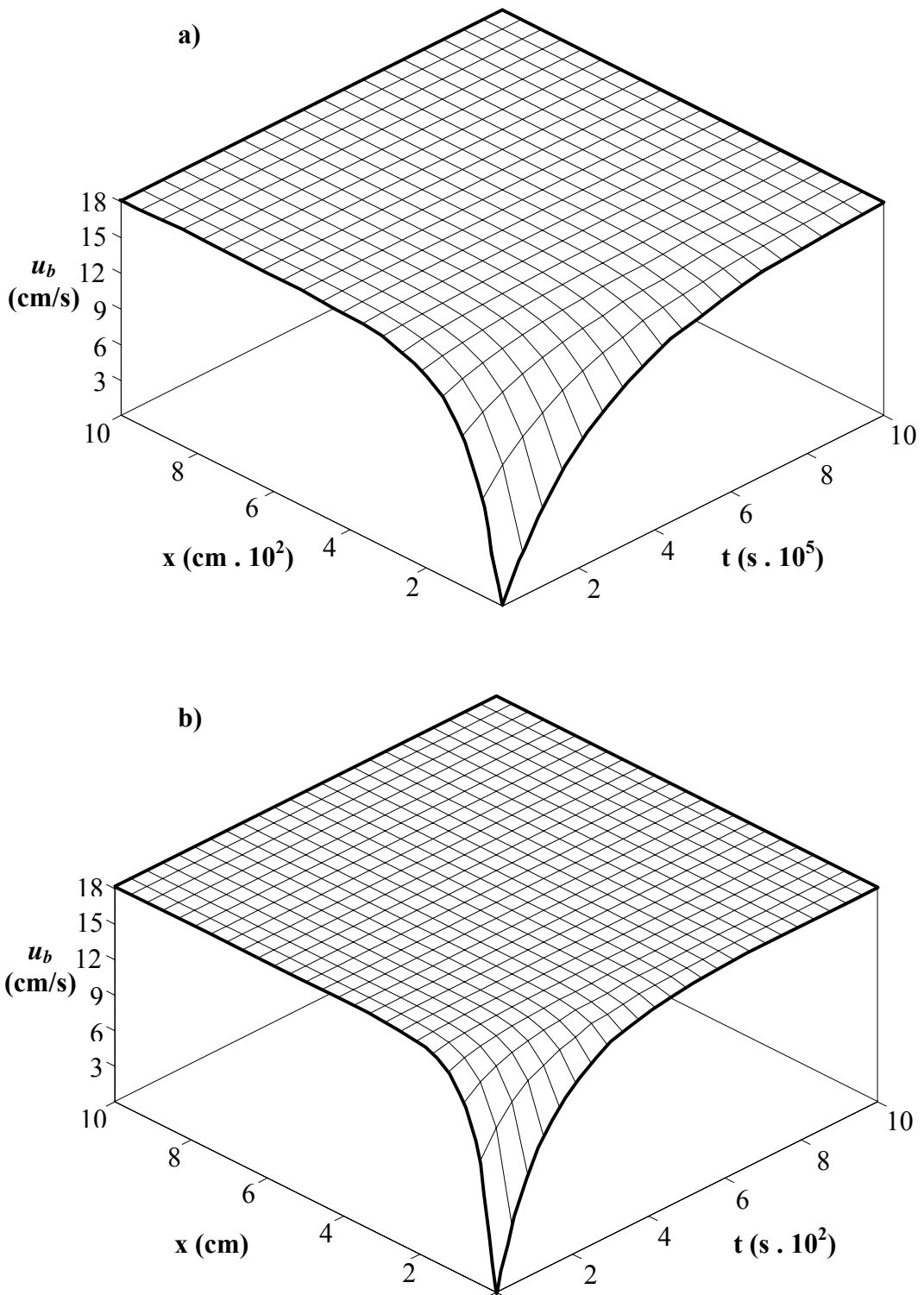


Figure 5.5. General trend of the unsteady state solution for $R_b=0.4$ cm (a) w/o added mass, (b) with added mass

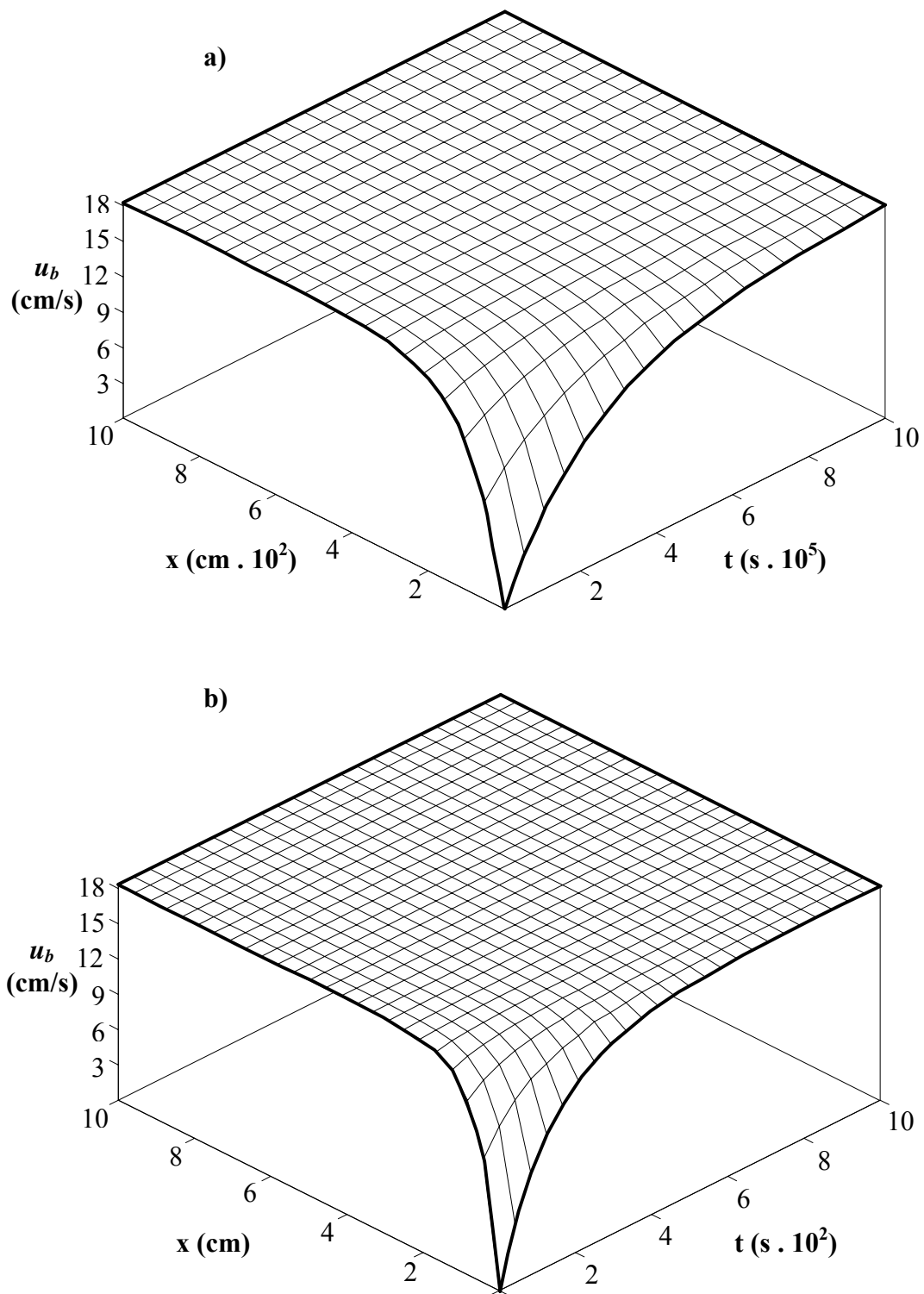


Figure 5.6. General trend of the unsteady state solution for $R_b=0.5$ cm (a) w/o added mass, (b) with added mass

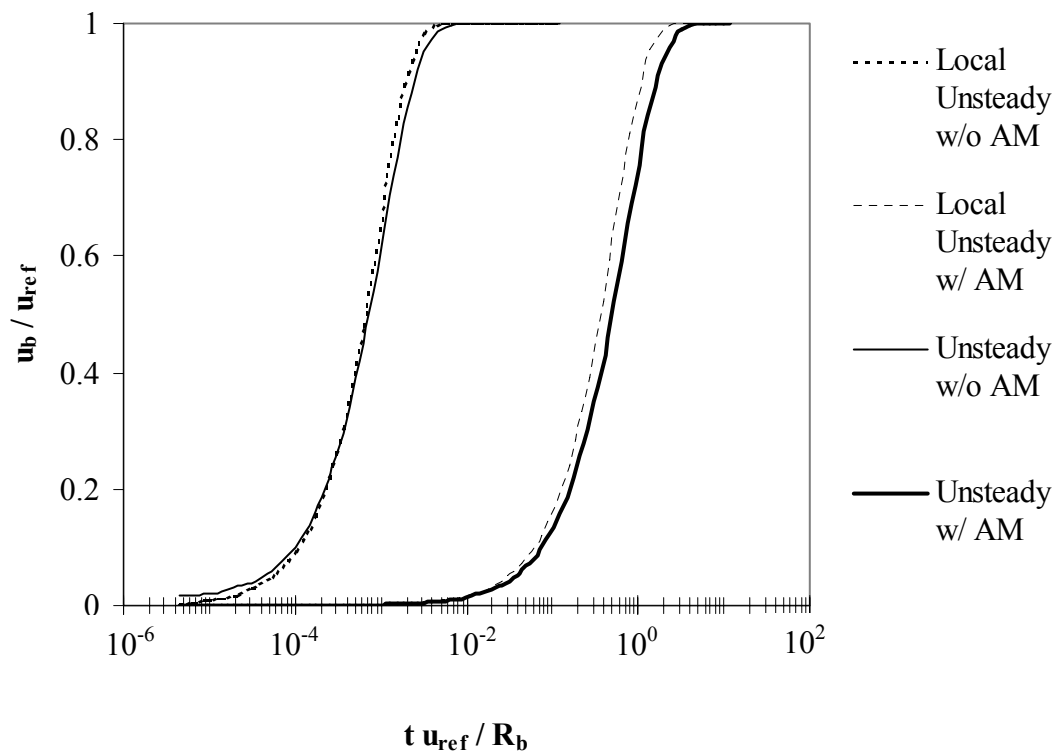


Figure 5.7. Normalized rise velocities at locally unsteady and unsteady flow conditions with and without the added mass force (AM)

CHAPTER 6

QUANTIFICATION OF FORCES

As noted earlier, the external forces acting on a bubble rising in a porous medium are the gravitational force, drag force, and surface tension. Since these forces are functions of the bubble radius as expressed by (2.3)-(2.5), they can be plotted varying with R_b as shown in Figure 6.1. The forces shown in the figure are calculated under steady state flow conditions. As seen in Figure 6.1, the total drag force takes up about 79 percent of the gravitational force for a bubble with $R_b=0.2$ cm. The rest is balanced by the surface tension. However, the contribution of the drag force increases with increasing bubble radius, and at about $R_b=0.3$ cm, the effect of surface tension on the total resistance force is negligible i.e., 6 % of the gravitational force. As seen in Figure 6.1, the contribution of kinetic energy losses to the total resistance force is almost equal to that of the viscous drag forces.

As explained earlier, the bubble's inertial force is supplemented when it moves relative to the surrounding liquid. The additional inertial force is to drag a mass of surrounding liquid with a volume equal to $(C_M \rho_f / \rho_g)$ percent of the bubble volume. The high density ratio of the surrounding liquid to the bubble gas makes the contribution of the added mass force quite significant at very early times of the bubble motion. Figures 6.2 and 6.3 illustrate the effect of "added mass" force compared to other forces on a rising bubble. In Figures 6.2 and 6.3,

all forces were normalized by the gravitational force shown in Figure 6.1. During the bubble's accelerated motion, the total drag force dominates the total resistance force for all bubbles. Initially, the contribution of the added mass force to the total resistance force constitutes 99 percent of the total resistance force for larger bubbles ($R_b=0.5$ cm) while this reduces to 79 percent for smaller bubbles ($R_b=0.2$ cm). The contribution of the added mass force declines very rapidly for bubbles of all sizes as the rise velocity reaches to the terminal velocity i.e., $Du_b/Dt \rightarrow 0$ at around $t=0.20$ sec. At that time, the effect of surface tension reduces to 1 percent for larger bubbles down from 21 percent for smaller bubbles.

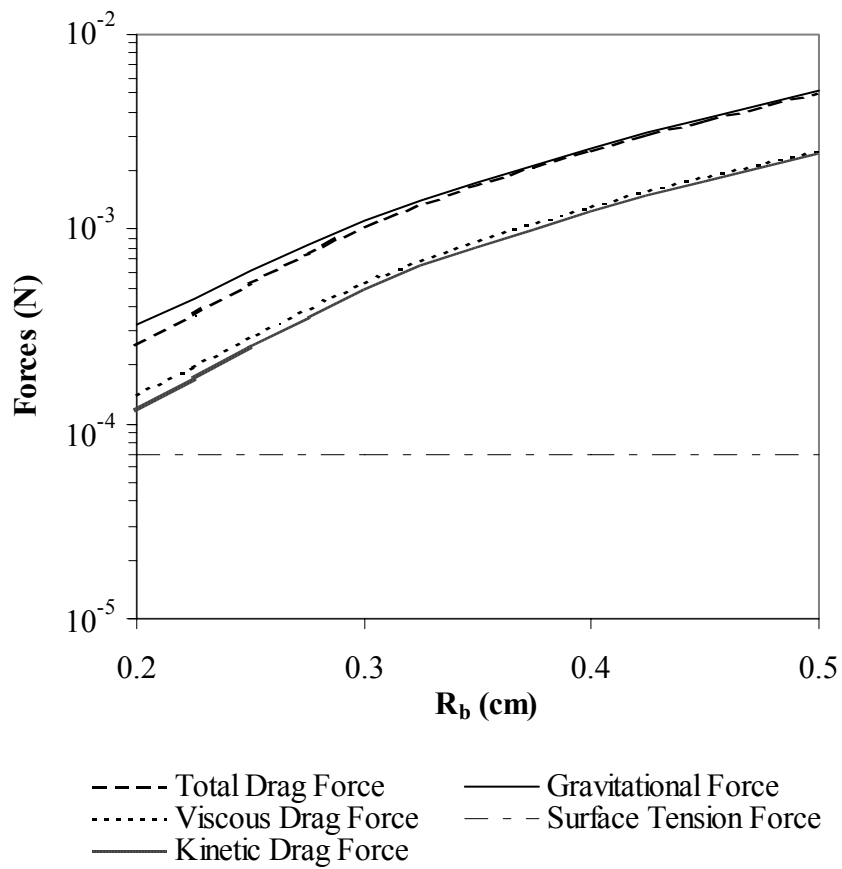


Figure 6.1. External forces at steady state

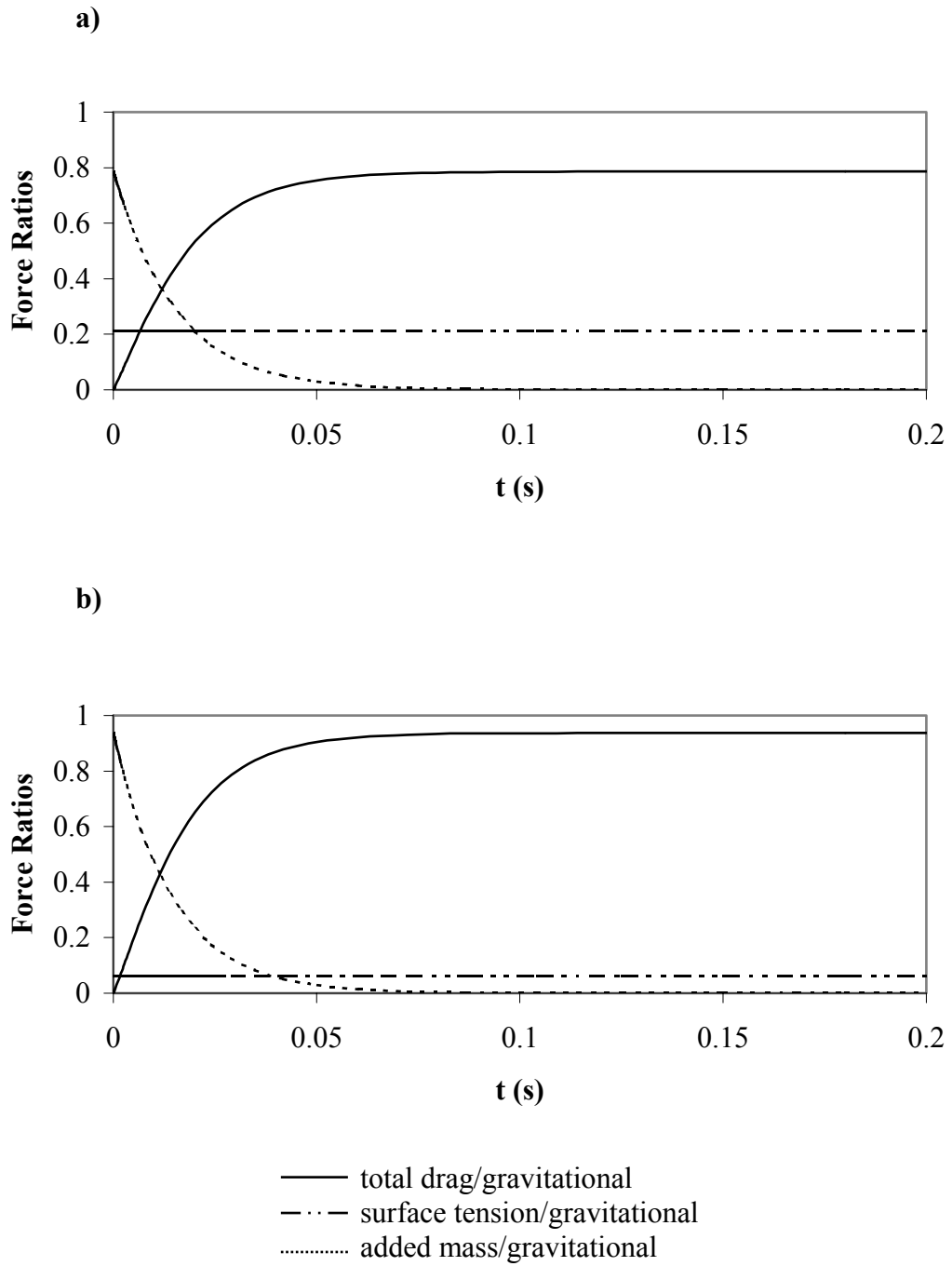


Figure 6.2. Temporal variation of force ratios for (a) $R_b=0.2$ cm and (b) $R_b=0.3$

cm

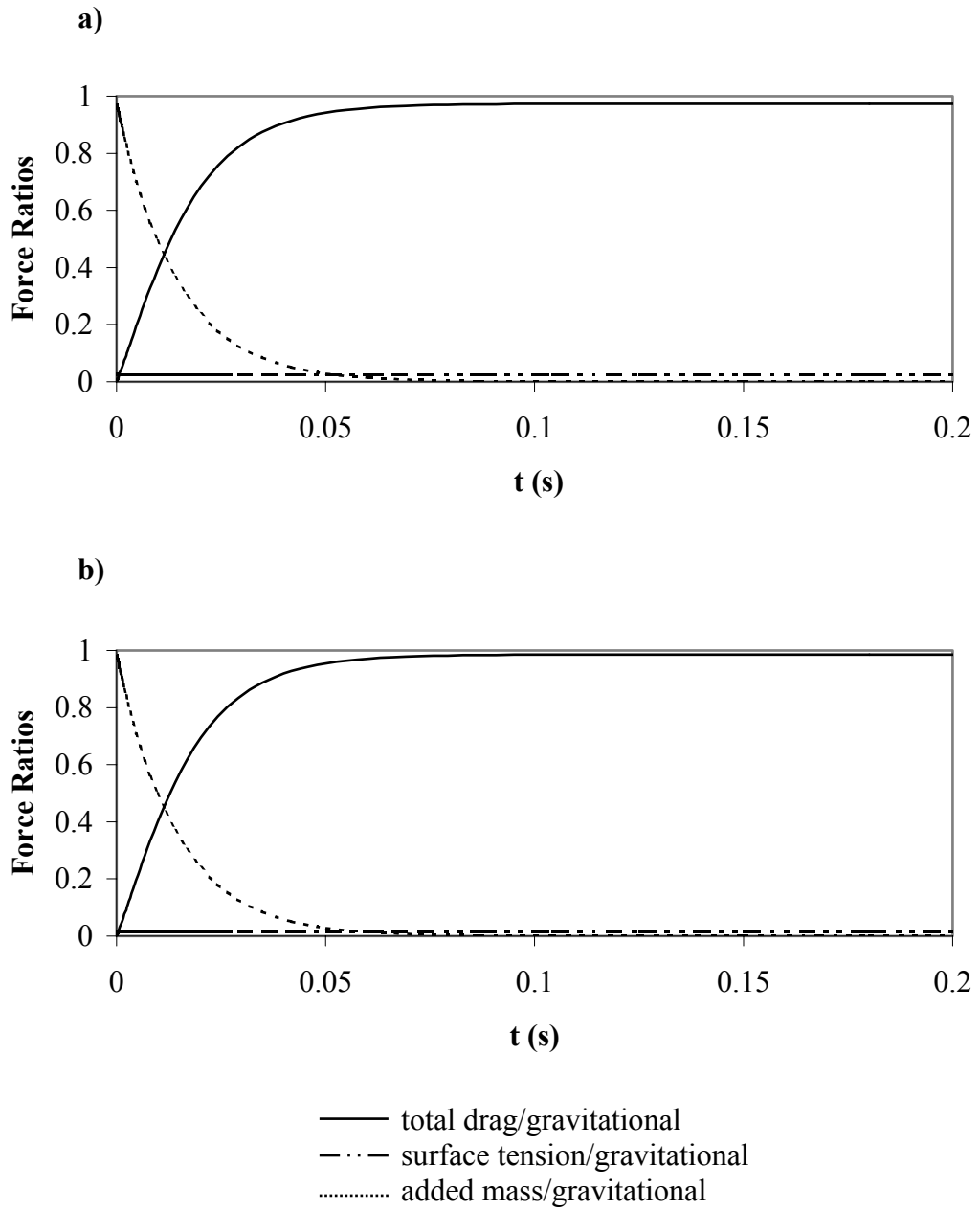


Figure 6.3. Temporal variation of force ratios for (a) $R_b=0.4$ cm and (b) $R_b=0.5$ cm

CHAPTER 7

DIMENSIONAL ANALYSIS

A dimensional analysis of the phenomenon can be conducted to provide a more generalized methodology to evaluate the effect of individual forces acting on an air bubble. Log-log scale plots, especially, reveal the functional dependence of one dimensionless group in response to orders of magnitude changes in another dimensionless group. The dimensional analysis is accomplished by substituting the dimensionless variables as $x^* = x/R_b$, $t^* = tu_{ref}/R_b$, and $u^* = u_b/u_{ref}$ in equation (2.6) and rearranging,

$$-D_2^2 u^{*2} - D_2^1 u^* - (D_3 - D_1) = A_d \left(\frac{\partial u^*}{\partial t^*} + u^* \frac{\partial u^*}{\partial t^*} \right) \quad (7.1)$$

The dimensionless coefficients D_1 , D_2^1 , D_2^2 , and D_3 are functions of the bubble radius and the terminal rise velocity. Since in this study, we are comparing bubbles of different sizes rising in a specific porous medium (i.e., $d_p = 4$ mm), the bubble radius is taken as the characteristic length in dimensionless numbers.

The dimensionless coefficient D_1 is the ratio of gravitational (buoyancy) to inertial forces and is inversely proportional to the square of the Froude number.

$$D_1 = \frac{(\rho_f - \rho_g)gR_b}{u_{ref}^2 \rho_g} = \frac{(\rho_f - \rho_g)}{\rho_g} \frac{1}{Fr^2} \quad (7.2)$$

The Froude number, Fr represents the ratio of inertial to gravitational forces. As shown in Figure 7.1, D_1 increases almost linearly with the bubble radius. For all values of R_b , gravitational forces dominate the inertial forces heavily.

The second dimensionless coefficient D_2 represents the ratio of drag forces to inertial forces.

$$D_2 = D_2^1 + D_2^2 = \frac{4020\mu_b(1-n)^2 R_b}{d_p^2 n^3 \rho_g u_{ref}} + \frac{46.9(1-n)R_b}{n^3 d_p} \quad (7.3)$$

The coefficient D_2 consists of two terms: the first component, D_2^1 , incorporates the linear viscous drag and the second component, D_2^2 , represents the kinetic effect of the bubble rise. As seen in Figure 7.1, a linear relation between D_2 and the bubble radius, R_b is very similar to the one obtained for D_1 . This clearly indicates that for bubbles with radii larger than 0.3 cm, the gravitational forces are balanced almost entirely by the drag forces. For bubbles with $R_b < 0.3$ cm, the surface tension has some contribution to balance the gravitational forces.

Then, we plot the ratio D_1/D_2 which describes the bubble rise when the density difference (buoyancy) provides the major driving force against the drag force, as a function of the bubble Reynolds number defined by $Re = 2u_b R_b \rho_f / \mu_f$. The ratio of D_1/D_2 is actually another representation of the ratio of the gravitational to viscous forces. On a log-log scale, Figure 7.3 shows

that for all bubbles, the relationship between the gravitational and inertial forces is a linear one.

The dimensionless coefficient D_3 is expressed by

$$D_3 = \frac{3 R' \sigma \sin\theta}{2 R_b^2 \rho_g u_{ref}^2} = \frac{3 R' 1}{2 R_b We} \quad (7.4)$$

D_3 is the ratio of surface tension to inertial force and is inversely proportional to the Weber number, which is the ratio of the inertial force to surface tension forces. Figure 7.1 shows that D_3 decreases with the bubble radius rapidly up to $R_b = 0.3$ cm and then the change in D_3 is quite small. Since the Weber number increases with bubble radius, it follows that the inertial forces are dominant for larger bubbles while surface tension characterize the motion of smaller ones. A plot of l/D_3 as a function of Re in Figure 7.3 reveals a linear relationship between these two dimensionless numbers characterizing the surface tension and the flow conditions, respectively.

In order to determine the relationship between the buoyancy and surface tension as a function of the bubble Reynolds number, we express D_1/D_3 as

$$\frac{D_1}{D_3} = \frac{2R_b^3 g (\rho_f - \rho_g)}{3R' \sigma \sin\theta} = \frac{2 R_b}{3 R'} Bo \quad (7.5)$$

Bo is the Bond number $\left[Bo = gR_b^2 (\rho_f - \rho_g) / \sigma \sin\theta \right]$, which presents the ratio of gravitational to surface tension forces. As expected, D_1/D_3 would increase very

rapidly with the bubble radius. Since the Bond number also increases with the bubble radius, the gravitational forces dominate more than the surface tension for larger bubbles.

A plot of D_2^1/D_3 can achieve a comparison of the ratio of the viscous drag force to surface tension. As discussed earlier, the Ergun equation we employed in this study to express the drag forces incorporates the kinetic energy losses as well as the viscous ones. Therefore, an analysis of D_2^1/D_3 rather than D_2/D_3 would separate the effect of viscous drag from that of the kinetic one. Then,

$$\frac{D_2^1}{D_3} = \frac{8040}{3} \left(\frac{(1-n)^2 R_b^3}{n^3 R' d_p^2} \right) \frac{\mu_b u_{ref}}{\sigma \sin\theta} = \frac{8040}{3} \left(\frac{(1-n)^2 R_b^3}{n^3 R' d_p^2} \right) Ca \quad (7.6)$$

where Ca is the capillary number which expresses the relative magnitude of viscous and capillary forces. As seen in Table 7.1, at larger velocities, the effect of viscous and kinetic losses are of an equivalent magnitude i.e., D_2^1 vs. D_2^2 while the effect of surface tension vanishing. However, for smaller bubbles, the effect of surface tension is almost equal to 50 percent of the viscous drag i.e., D_3 vs. D_2^1 . As noted earlier, $R_b = 0.3$ cm is the threshold value for the bubble radii to neglect the effect of surface tension on the total resistance force.

Table 7.1. Results of dimensional analysis

bubble	measured	theoretical					
radius	terminal	terminal					
R_b	bubble	bubble	D_1	D_2^1	D_2^2	D_2	D_3
(cm)	velocity u_b	velocity u_b					
	(cm/s)	(cm/s)					
0.2	17.15	15.71	643.62	276.76	229.35	506.11	137.51
0.3	16.80	17.70	760.68	368.50	344.03	712.52	48.16
0.4	17.80	18.16	963.25	478.82	458.70	937.52	25.73
0.5	18.30	18.32	1182.76	593.21	573.38	1166.58	16.18

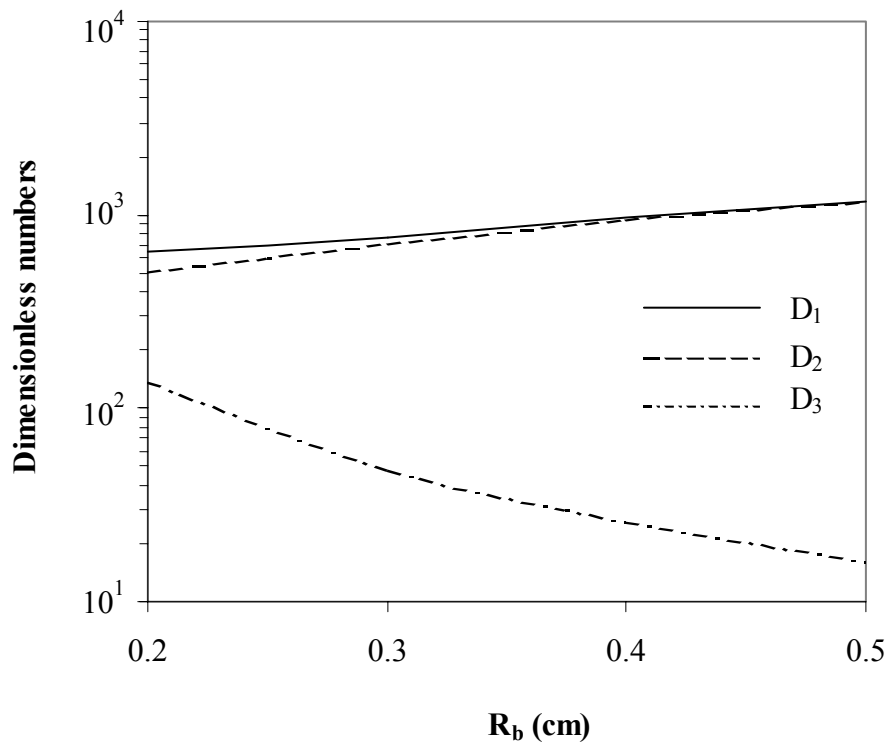
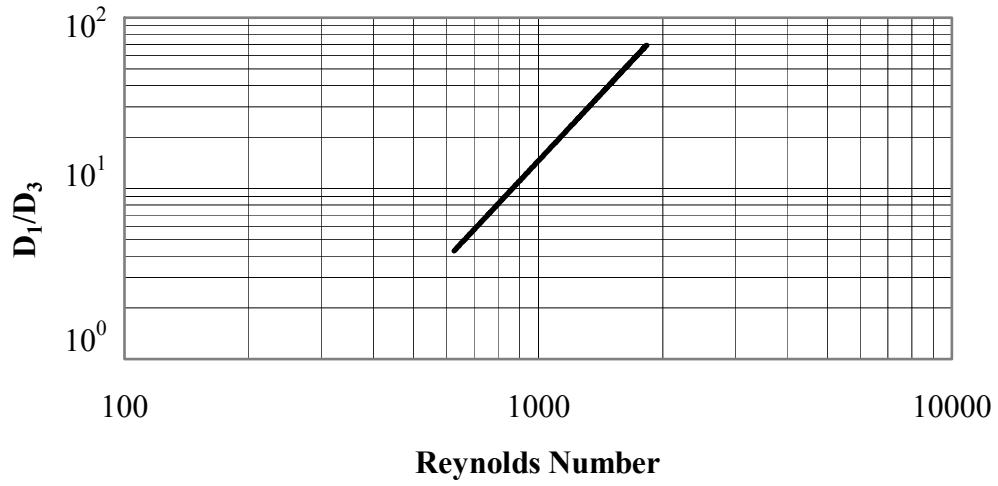


Figure 7.1. Dimensionless numbers as functions of the equivalent bubble radius

a)



b)

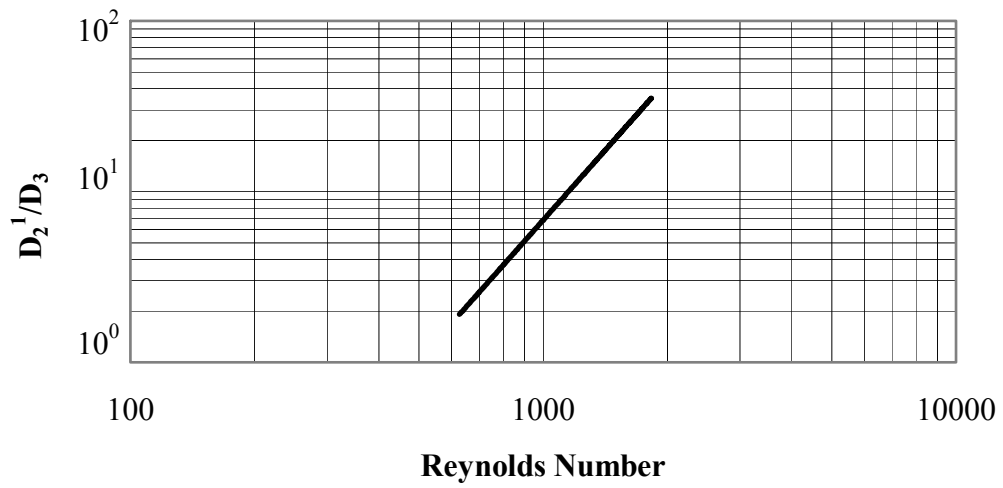
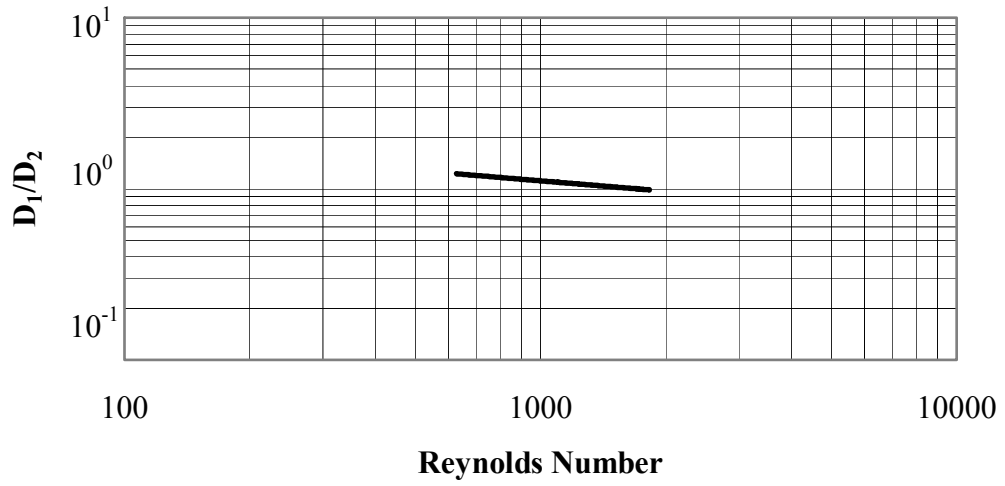


Figure 7.2. Ratio of dimensionless number a) D_1/D_3 and b) D_2^1/D_3 as functions of the bubble Reynolds number, Re

a)



b)

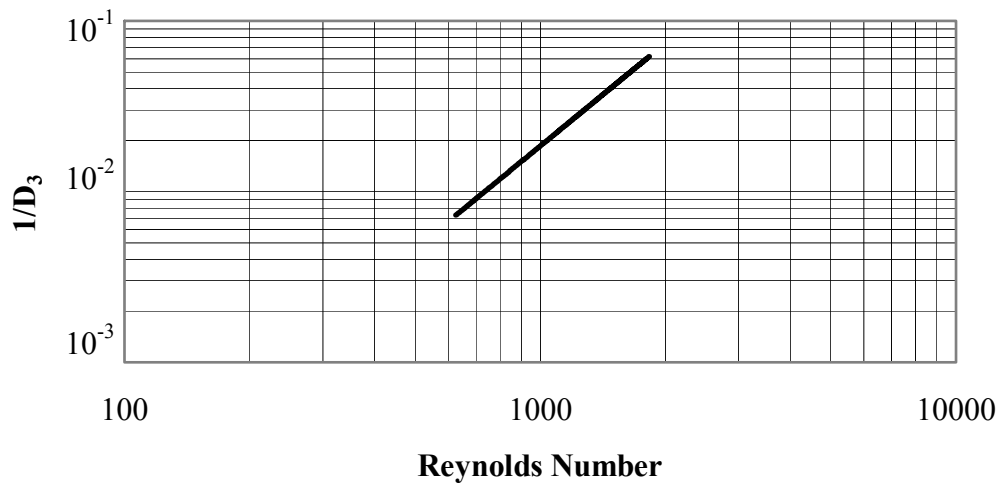


Figure 7.3. Ratio of dimensionless number a) D_1/D_2 and b) $1/D_3$ as functions of the bubble Reynolds number, Re

CHAPTER 8

SUMMARY AND CONCLUDING REMARKS

The airflow in coarse porous media can be observed in the form of discrete air bubbles. The objective of this study is to present a theoretical framework to analyze the rise velocity of a single air bubble in otherwise water saturated porous medium. The results of a dimensional analysis presented in Table 7.1 and Figures 7.1-7.3 show that for larger bubbles, the total drag force more than by any other force balances the buoyant force while the surface tension has some effect for smaller bubbles. Results show that air bubbles rising in a porous medium equilibrate after a short travel time and very short distances of rise. Since the value of the total inertial force for all bubble velocities is negligible i.e., $A_d Du^* / Dt^* \approx 0$, the motion of an air bubble rising in a porous medium can be assumed as a steady state flow. The model developed here is subject to various assumptions including the assumption of gas incompressibility. *Roosevelt and Corapcioglu* [1998] have calculated that in a 1-m water saturated porous medium, bubble radii can increase by 5 % due to gas expansion. Another assumption is the negligibility of the local water flow around a bubble rising in a stagnant water phase. However, if the water phase has a pressure gradient that is not negligible, equations (2.6) and (2.5) should incorporate the bubble velocity relative to that of the water phase.

REFERENCES

- Brooks, M. C., W. R. Wise, and M. D. Annable, Two- phase flow patterns in porous media: An investigation relating to in-situ air sparging, Proc. First Int. Symp. on In-situ Air Sparging for Site Remediation, Oct. 24-25, 1996, Las Vegas, NV.
- Ergun, S., Fluid flow through packed columns. Chem. Eng. Prog., 48(2), 89-94, 1952.
- Garrettson, B. A., Bubble transport theory with application to the upper ocean, J. Fluid Mech., 59(1), 187-206, 1973.
- Graton, L. C., and H. J. Fraser, Systematic packing of spheres with particular relation to porosity and permeability, The Journal of Geology, 43(8), 803, 1935.
- Gvirtzman, H. and S. M. Gorelick, The concept of in-situ vapor stripping for removing VOCs from groundwater, Transport in Porous Media, 8, 71-92, 1992.
- Ji, W. A. Dahmani, D. P. Ahlfeld, J. D. Lin, and E. Hill III, Laboratory study of air sparging: Air flow visualization, Ground Water Monitoring and Remediation, 13(4), 115-126, 1993.
- Kovscek, A. R., and C. J. Radke, Fundamentals of foam transport in porous media, in Foams edited by L. L. Schramm, pp. 115-163, American Chemical Society, Washington, DC, 1994.

- Levich, V. G., *Physicochemical Hydrodynamics*, Prentice-Hall, Englewood Cliffs, N. J., 1962.
- Loubiere, K. and G. Hebrard, Bubble formation from a flexible hole submerged in an inviscid liquid, *Chem. Eng. Sci.*, 58, 135-148, 2003.
- Massmann, J. W., Applying groundwater models in vapour extraction system design. *J. Environ. Eng.*, 115(1), 129-149, 1989.
- Ortiz-Arroyo, A., F. Larachi, and I. Iliuta, Method for inferring contact angle and for correlating static liquid hold-up in packed beds, *Chem. Eng. Sci.*, 58, 2835-2855, 2003.
- Pankow, J. F., R. L. Johnson, and J. A. Cherry, Air sparging in gate wells in cutoff walls and trenches for control of plumes of volatile organic compounds (VOCs) *Ground Water*, 31(4), 1993.
- Roosevelt S. E., M. Y. Corapcioglu, Air bubble migration in a granular porous medium: Experimental studies, *Water Resour. Res.*, 34(5), 1131-1142, 1998.
- Semer, R., J. A. Adams and K. R. Reddy, An experimental investigation of air flow patterns in saturated soils during air sparging, *Geotechnical and Geological Engineering*, 16, 59-75, 1998.
- Soubiran, J., and J. D. Sherwood, Bubble motion in a potential flow within a venturi, *Int. J. Multiphase Flow*, 26, 1171-1796, 2000.
- Wallis, G. B., *One-dimensional two-phase flow*, pp. 219, McGraw-Hill, New York, 1969.
- Wehrle, K., In-situ cleaning of CHC contaminated sites: Model-scale experiments using the air injection method in granular soils, in *Contaminated Soil' 90*,

ed. F. Arendt, M. Hinsenfeld and W. J. van den Brink, pp. 1061-1062,
Kluwer, the Netherlands, 1990.

Zhang, J., and L. S. Fan, On the rise velocity of an interactive bubble in liquids,
Chem. Eng. J., 92, 169-176, 2003.

APPENDIX A

NOTATION

ΣF	Sum of external forces acting on a single air bubble, N
\forall_b	Volume of a bubble, m ³
$\frac{D}{Dt}$	Material derivative, t ⁻¹
t	Time, s
x	Depth in the vertical direction, m
u_b	Bubble rise velocity, m/s
u_{ref}	Terminal bubble velocity, m/s
R_b	Equivalent bubble radius, m
F_b	Buoyancy (gravitational) force, N
F_d	Drag force, N
F_{st}	Surface tension force, N
g	Gravity acceleration, m/s ²
n	Porosity
d_p	Grain diameter, m
R'	Radius of a pore throat, m

n_b	Number of bubbles per unit volume of air, $1/\text{m}^3$
A	Correction factor, dimensionless
A_d	Terminal velocity delay index, dimensionless
C_M	Added mass coefficient, dimensionless
c	Empirical constant, dimensionless
t^*	Dimensionless time
x^*	Dimensionless depth
u^*	Dimensionless bubble rise velocity

Greek Letters

ρ_g	Density of air, kg/m^3
ρ_f	Density of fluid (water), kg/m^3
σ	Surface tension, N/m
θ	Contact angle, $^\circ$
μ_b	Effective bubble dynamic viscosity, $\text{N}\cdot\text{s}/\text{m}^2$
μ_g	Dynamic viscosity of air, $\text{N}\cdot\text{s}/\text{m}^2$
μ_f	Dynamic viscosity of fluid (water), $\text{N}\cdot\text{s}/\text{m}^2$
α	Proportionality constant, $\text{N}\cdot\text{m}^{7/3}/\text{s}^{2/3}$

Dimensionless Numbers

D_1	The ratio of gravitational force to inertial force
D_2	The ratio of drag force to inertial force

D_2^1 The ratio of linear viscous drag force to inertial force

D_2^2 The ratio of kinetic drag force to inertial force

D_3 The ratio of surface tension force to inertial force

Fr Froude number $\left[\frac{u_b}{\sqrt{gR_b}} \right]$, the ratio of inertial force to gravitational force

Re Reynolds number $\left[\frac{2R_b u_b \rho_f}{\mu_f} \right]$, the ratio of inertial force to viscous force

We Weber number $\left[\frac{u_b^2 \rho_f R_b}{\sigma \sin \theta} \right]$, the ratio of inertial force to surface tension force

Bo Bond number $\left[\frac{gR_b^2 (\rho_f - \rho_g)}{\sigma \sin \theta} \right]$, the ratio of gravitational force to surface tension

Ca Capillary number $\left[\frac{\mu_b u_{ref}}{\sigma \sin \theta} \right]$, the ratio of viscous force to surface tension force

APPENDIX B

TERMINAL VELOCITY MEASUREMENT OF AN AIR BUBBLE IN COARSE POROUS MEDIA

In the experimental work conducted by *Roosevelt and Corapcioglu* [1998] of which the results were compared with the theoretical ones obtained in this study, a vertically mounted cylindrical glass column filled with transparent 4-mm glass beads and fully saturated with distilled water simulated a coarse granular porous medium (Figure B1). The cylindrical column was filled with ~90 cm of beads which are covered by an additional 10 cm of water. A random packing procedure was used to deposit the 4-mm beads and average porosity of 0.39 was found by measuring the volumes of the total sample and of the solid matrix when the beads were added to the water-filled 3.9-cm-diameter column.

Two different air injection methods were employed in the experimental work of *Roosevelt and Corapcioglu* [1998]. In the first method as shown in Figure B1a, compressed air was injected into the base of the larger column through the use of an electronically controlled solenoid valve. A WavetekeTM sweep generator sends a single voltage pulse of preset length through a series of relay circuits to open the normally closed solenoid valve and thus allow a single air bubble to enter a tube leading to the column. The second method for introducing bubbles was depicted in Figure B1b. Air was injected by hand into the base of the smaller

column with a 19-gauge hypodermic needle and a 3-cc (cubic centimeters) syringe. The needle was inserted into the beads through a septum at the top of an 8-mm-inner-diameter orifice. This technique yielded smaller individual bubbles in the porous medium than the first method.

In both methods the bubbles were injected along the column axis. Measurements were made at room temperature ($\sim 24^{\circ}\text{C}$), and the column has open tops. To provide contrast between the air bubble and water, McCormickTM blue food dye has been added to most of the experiments to make the visualization of the bubble in the porous medium with the image analyzer easier.

To aid in the visualization of the bubble, the column was lit from behind by a vertical fluorescent light source situated ~ 100 cm away. The bubble motion through the column was recorded by two JVCTM Videomovie VHSC camcorders. The rise of a bubble was timed by an Atec, Inc.TM timing device with a neon plasma display, which is independent of room lighting. In order for the time to be visible on the videotape to an accuracy of 0.1 s, a magnifying glass was placed in front of the timer. To obtain an image of a rising bubble in the porous medium, a still frame from the videotape was captured and enhanced with an image analyzer. The images were viewed on a Sony Trinitrone color video monitor, and the analysis was performed using Image-Pro Pluse software.

The rate of vertical rise of the bubbles was determined by measuring the displacement of the center of a bubble from the top of the porous medium in the enhanced images [see *Roosevelt and Corapcioglu*, 1998]. These displacements were plotted against time and displayed a linear dependence. The rise velocity was then computed by applying a linear best fit to these data. The bubble radius is the

equivalent radius of the bubble just after it exits the porous medium. It was determined using the main camcorder by capturing still frames of the bubble in the water above the beads.

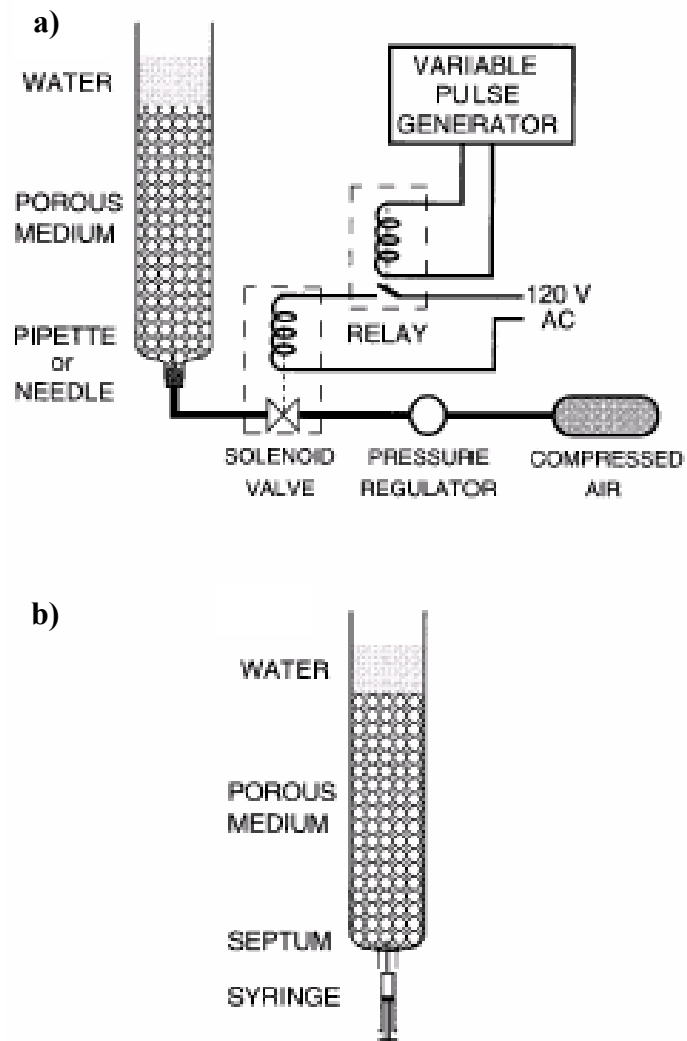


Figure B1. Experimental apparatus (after *Roosevelt and Corapcioglu, 1998*)